NBS TECHNICAL NOTE 678

U. S. DEPARTMENT OF COMMERCE / National Bureau of Standards

An Electrically Calibrated Pyroelectric Radiometer System

NATIONAL BUREAU OF STANDARDS

The National Bureau of Standards[1] was established by an act of Congress March 3, 1901. The Bureau's overall goal is to strengthen and advance the Nation's science and technology and facilitate their effective application for public benefit. To this end, the Bureau conducts research and provides: (1) a basis for the Nation's physical measurement system, (2) scientific and technological services for industry and government, (3) a technical basis for equity in trade, and (4) technical services to promote public safety. The Bureau consists of the Institute for Basic Standards, the Institute for Materials Research, the Institute for Applied Technology, the Institute for Computer Sciences and Technology, and the Office for Information Programs.

THE INSTITUTE FOR BASIC STANDARDS provides the central basis within the United States of a complete and consistent system of physical measurement; coordinates that system with measurement systems of other nations; and furnishes essential services leading to accurate and uniform physical measurements throughout the Nation's scientific community, industry, and commerce. The Institute consists of the Office of Measurement Services, the Office of Radiation Measurement and the following Center and divisions:

Applied Mathematics — Electricity — Mechanics — Heat — Optical Physics — Center for Radiation Research: Nuclear Sciences; Applied Radiation — Laboratory Astrophysics[2] — Cryogenics[2] — Electromagnetics[2] — Time and Frequency[2].

THE INSTITUTE FOR MATERIALS RESEARCH conducts materials research leading to improved methods of measurement, standards, and data on the properties of well-characterized materials needed by industry, commerce, educational institutions, and Government; provides advisory and research services to other Government agencies; and develops, produces, and distributes standard reference materials. The Institute consists of the Office of Standard Reference Materials, the Office of Air and Water Measurement, and the following divisions:

Analytical Chemistry — Polymers — Metallurgy — Inorganic Materials — Reactor Radiation — Physical Chemistry.

THE INSTITUTE FOR APPLIED TECHNOLOGY provides technical services to promote the use of available technology and to facilitate technological innovation in industry and Government; cooperates with public and private organizations leading to the development of technological standards (including mandatory safety standards), codes and methods of test; and provides technical advice and services to Government agencies upon request. The Institute consists of the following divisions and Centers:

Standards Application and Analysis — Electronic Technology — Center for Consumer Product Technology: Product Systems Analysis; Product Engineering — Center for Building Technology: Structures, Materials, and Life Safety; Building Environment; Technical Evaluation and Application — Center for Fire Research: Fire Science; Fire Safety Engineering.

THE INSTITUTE FOR COMPUTER SCIENCES AND TECHNOLOGY conducts research and provides technical services designed to aid Government agencies in improving cost effectiveness in the conduct of their programs through the selection, acquisition, and effective utilization of automatic data processing equipment; and serves as the principal focus within the executive branch for the development of Federal standards for automatic data processing equipment, techniques, and computer languages. The Institute consists of the following divisions:

Computer Services — Systems and Software — Computer Systems Engineering — Information Technology.

THE OFFICE FOR INFORMATION PROGRAMS promotes optimum dissemination and accessibility of scientific information generated within NBS and other agencies of the Federal Government; promotes the development of the National Standard Reference Data System and a system of information analysis centers dealing with the broader aspects of the National Measurement System; provides appropriate services to ensure that the NBS staff has optimum accessibility to the scientific information of the world. The Office consists of the following organizational units:

Office of Standard Reference Data — Office of Information Activities — Office of Technical Publications — Library — Office of International Relations — Office of International Standards.

---

[1] Headquarters and Laboratories at Gaithersburg, Maryland, unless otherwise noted; mailing address Washington, D.C. 20234.

[2] Located at Boulder, Colorado 80302.

An Electrically Calibrated Pyroelectric Radiometer System

C. A. Hamilton
G. W. Day
R. J. Phelan, Jr.

Electromagnetics Division
Institute for Basic Standards
National Bureau of Standards
Boulder, Colorado 80302

U.S. DEPARTMENT OF COMMERCE, Elliot L. Richardson, Secretary
James A. Baker, III, Under Secretary
Dr. Betsy Ancker-Johnson, Assistant Secretary for Science and Technology

NATIONAL BUREAU OF STANDARDS, Ernest Ambler, Acting Director

Issued March 1976

NATIONAL BUREAU OF STANDARDS TECHNICAL NOTE 678
Nat. Bur. Stand. (U.S.), Tech Note 678, 50 pages (Mar. 1976)

CODEN: NBTNAE

FOREWORD

The program to develop an Electrically Calibrated Pryoelectric Radiometer began in 1972 when Robert Phelan, Jr. demonstrated the first electrically calibrated pyroelectric detector. The potential of this device as an absolute radiometric standard was quickly realized, and a dual development effort began. The first part of this effort was aimed at characterizing and improving the detector itself while the second part involved the design of a complete radiometric instrument. The result of these efforts is the instrument described in this Technical Note.

The authors are grateful to Paul Gruzensky for his contribution to the understanding of pyroelectricity in PVF_2, to Lou Mullen for fabrication of detectors, to Gerry Klein and Kurt Pyatt for automating many of the characterization experiments and to Robert Peterson for his theoretical analysis of heat flow in pyroelectric detectors. The suggestions of Bill Blevin of the National Standards Laboratory, Australia, were crucial to our understanding and use of gold black absorbers. Finally we acknowledge the many ideas and incentive resulting from our interaction with Jon Geist of the Radiometry Section of NBS.

Contents

List of Figures

List of Figures (Continued)

AN ELECTRICALLY CALIBRATED PYROELECTRIC RADIOMETER SYSTEM

C.A. Hamilton, G.W. Day, and R.J. Phelan, Jr.

Abstract

A new type of radiometer based on an electrically calibrated pyroelectric detector is described. Emphasis is placed on system design and analysis with careful consideration of design trade-offs. An evaluation of both systematic and random errors for the complete system yields an expression for the accuracy relative to the electrical standards by which it is calibrated. Throughout the paper the analysis should be sufficiently general that it can be applied to any Electrically Calibrated Pyroelectric Radiometer which employs the same basic principals.

Key words: Detector; pyroelectric; radiometry.

1. Introduction

Until recently, most low level radiometric measurements have been based on standard sources such as blackbodies and standard lamps. The development of electrically calibrated pyroelectric detectors for low level power measurements has made possible a new standard which is based on a detector rather than on a source. This detector based standard uses a thermal detector whose response is nearly identical for optical power absorbed in its receiving surface and electrical power dissipated in that same surface. Thus optical power measurements can be translated directly into the units of electrical power. Since electrical standards are highly accurate and readily available in most laboratories, calibration is a simple and straightforward procedure. The design and theory of operation of these detectors has been described in numerous publications [1-8].

Figure 1.1 provides a brief review of the detector construction and operation. A pyroelectric material is sandwiched between two conducting electrodes. The front electrode is a gold black coating which is both highly absorbing and electrically conductive. The pyroelectric material contains an electric dipole moment which is a function of temperature. Thus, when it is heated, the induced charge on the surface electrodes changes and a current flows to the preamplifier. The heat input may come either from optical radiation absorbed in the "black" or from electrical power dissipated in the "black." The electrical power is used for calibration and is determined using a four wire measurement of the voltage and current at the heater. The detector produces an output only when its temperature is changing, thus the input power must always be chopped.

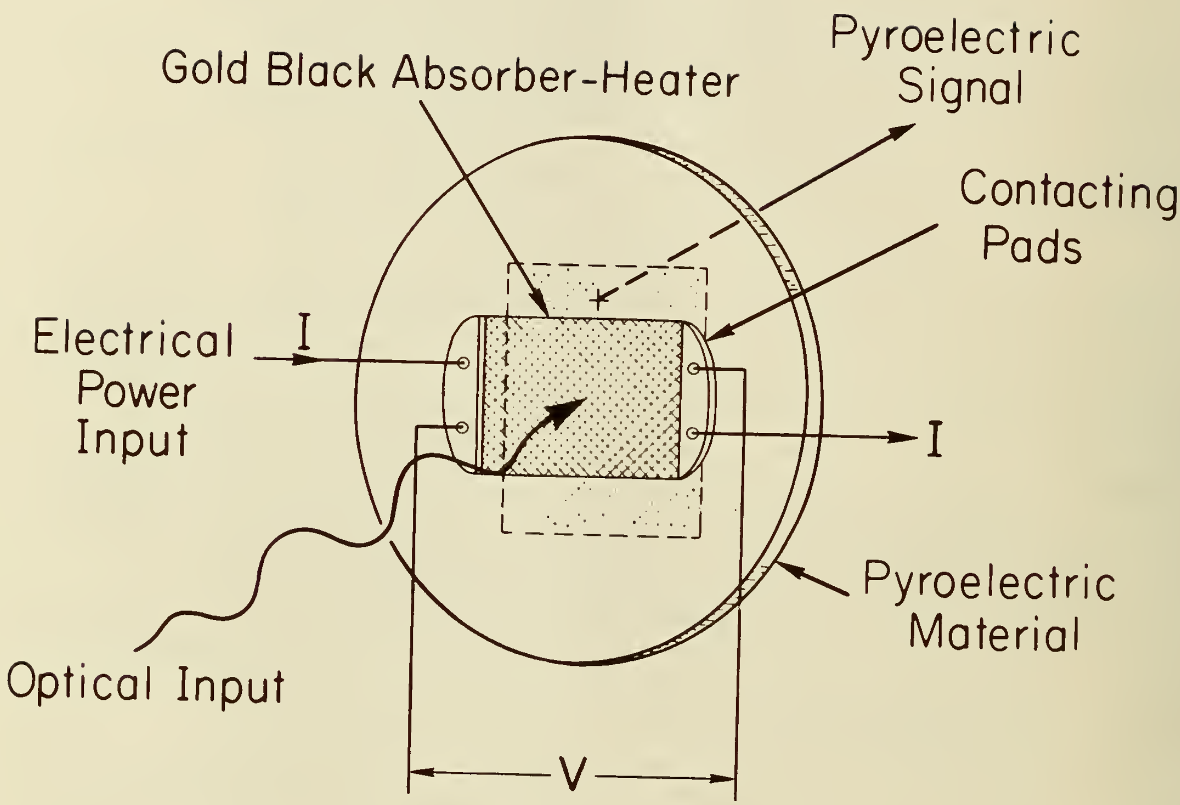

Figure 1.1 A schematic diagram of the pyroelectric detector shows how the gold black functions as both optical absorber and electrical heater.

This technical note will cover in detail the operation of a complete Electrically Calibrated Pyroelectric Radiometer (ECPR) system based on one of these detectors. The next section uses a block diagram approach to describe the entire system. Section 3 provides an analysis of the circuits which make up each block. Emphasis will be placed on identifying design trade offs and justifying the particular design choices made. Section 4 is a careful analysis of all the known sources of error. It takes into account the non-ideal nature of all of the system components in order to arrive at a realistic evaluation of the total system error.

2. System Operation

Figure 2.1 is a block diagram of the complete system. The incident radiation to be measured is chopped with a mechanical chopper and absorbed in the detector surface. During the time the radiation is blocked, an electrical signal is synchronously applied across the heater on the detector surface. The detector response to the optical and electrical heat input is amplified and synchronously demodulated in such a way that the lock-in amplifier output is proportional to the difference between the optical and electrical inputs. This difference signal is fed back around a closed servo loop to drive the electrical input thus reducing the difference signal to zero. Hence, the electrical input tracks the optical input and a continuous balance is maintained.

The lower half of figure 2.1 shows how the electrical power is computed and displayed. The voltage and current for the detector heater are measured with a pair of differential amplifiers. The outputs of these amplifiers are multiplied together with a high accuracy analog multiplier and the resulting power is displayed in 3 1/2 digits.

The null balance technique used in this system takes advantage of the speed and sensitivity of pyroelectrics and yet is independent of changes in detector responsivity or amplifier gain. Calibration does not depend on any standard optical source but rather is based directly on readily available electrical standards. The realization of such a system requires solutions to a number of practical problems. Before going into the detailed design, we shall consider four of the most important of these problems and the design choices made to solve them.

The first problem results from the fact that the electrical and optical waveforms and phase are not necessarily identical. The electrical waveform is a square wave with finite rise and fall times. It is convenient to define its phase to be zero. The waveform and phase of the optical signal, however, are determined by the irradiance distribution over the chopper aperture. One method of matching the electrical and optical signals is to equate the integrated power due to each signal. This approach requires the use of a 25%

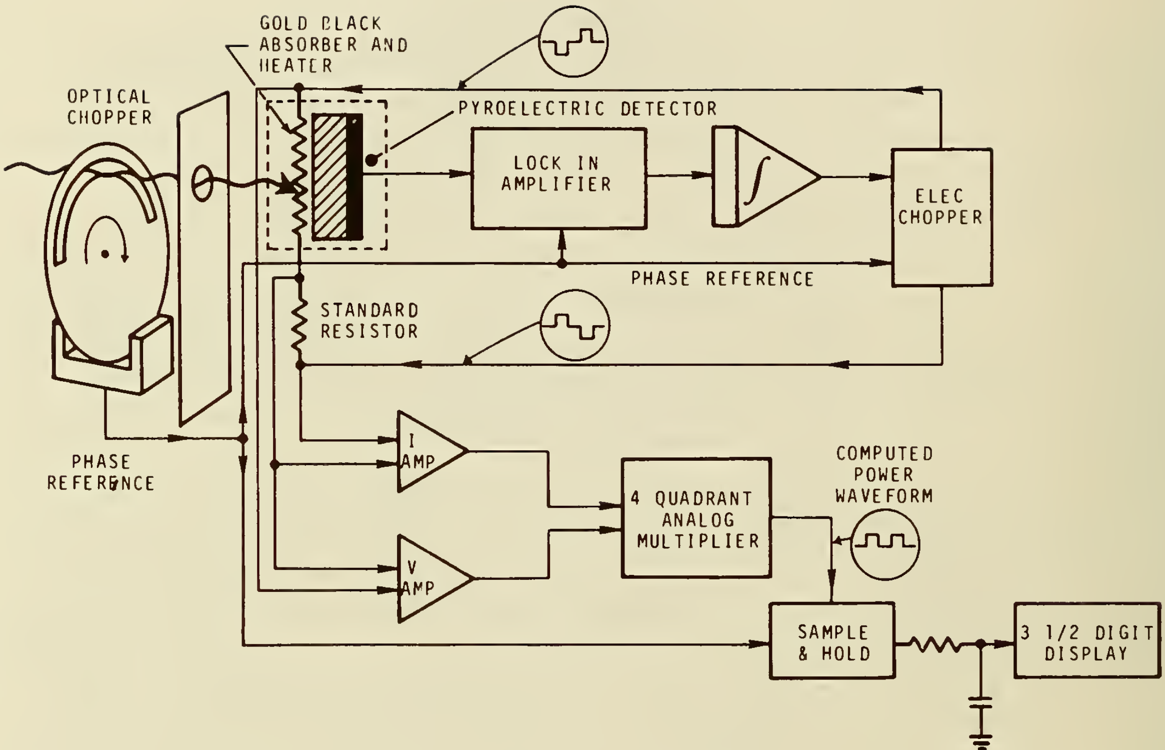

Figure 2.1 Block diagram of the Electrically Calibrated Pyroelectric Radiometer (ECPR) shows the null balance servo loop (upper portion) and power computing circuitry (lower portion).

duty cycle and a wide band lock-in amplifier following the detector output and is usually referred to as the waveform independent method [9]. In theory, this method yields equivalence regardless of the optical waveform but it has the disadvantage of requiring exactly matched electrical-optical duty cycles and a complex wide-band front end amplifier with a very large dynamic range.

Our approach is to use a 50% duty cycle and a narrow band lock-in amplifier so that only the fundamental, in phase, components of the electrical and optical signals are matched. This approach leads to a small dependence on the irradiance distribution over the chopper aperture. With a proper chopper design the resulting worst case error is easily held to less than a few tenths of a percent. In addition to the advantages of simplicity, this method yields a 2:1 improvement in signal-to-noise and is relatively insensitive to such practical problems as the electrical power turn on transient and small deviations in the relative lengths of the electrical and optical duty cycles. A quantitative evaluation of all of these error sources is made in Section 4.

Another problem arises from the fact that the voltage across the detector heater resistance is capacitively coupled directly into the detector output. Two solutions are diagrammed in figure 2.2. The first is to introduce an insulating layer and a ground plane between the heater and the pyroelectric material. The ground plane serves as the front electrode for the detector and simultaneously shields the detector from the heater. Unfortunately, this method has the disadvantage of complicating detector fabrication and making it very difficult to achieve uniform response over the detector surface.

The approach we are using is to drive opposite ends of the heater with equal and opposite voltages, thus establishing a virtual ground at the center of the heater. This causes the capacitively coupled signals to cancel. Any residual error caused by the imprecise adjustment of this virtual ground is further reduced by reversing the heater voltage every other cycle. Capacitively coupled signals are thus at one-half the chopper frequency and are rejected by the lock-in amplifier.

This reversal of the heater voltage every other cycle has a further important function in the calculation of the electrical power. Since the voltage and current waveforms are maintained throughout the power calculation circuitry, any zero offsets in either the drive or calculation circuits will, to first order, cancel out in the final filter before the display. This feature significantly improves the accuracy and temperature stability of the power calculation. A detailed error calculation for the power computation circuitry is given in section 4.

The third design problem to be considered is the servo loop which automatically balances the electrical and optical power. This loop, shown in figure 2.3, consists of the detector, whose output is proportional to the

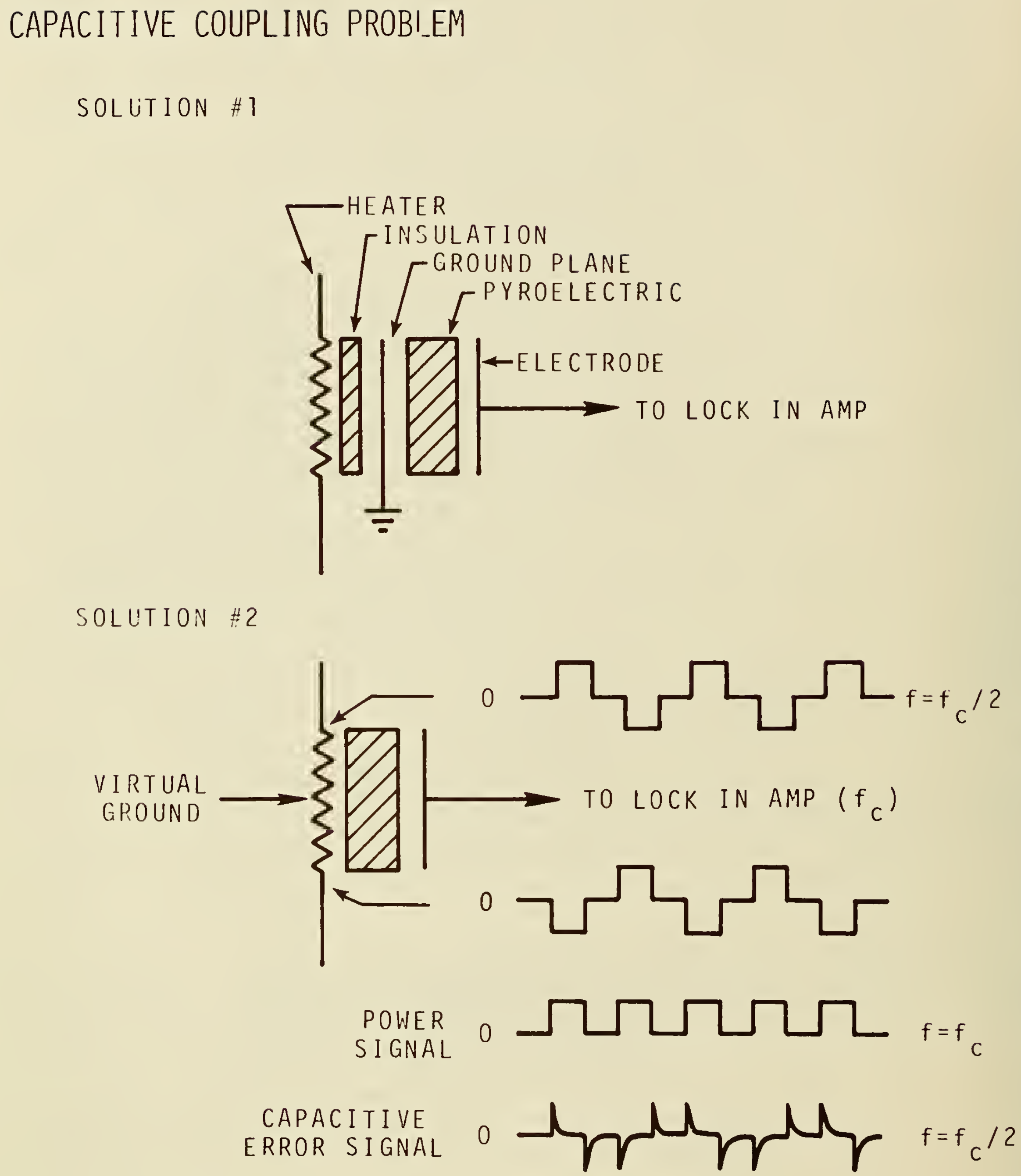

Figure 2.2 Capacitive coupling from the heater to the detector output can be corrected by (1) shielding or (2) cancellation.

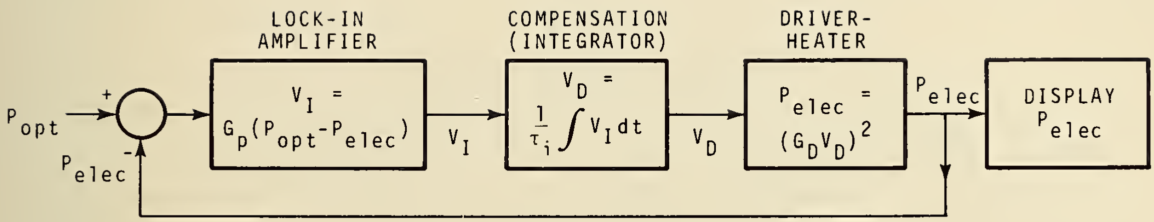

Figure 2.3 A system diagram of the null balance servo loop. The nonlinear behavior of the loop gives rise to a time constant which continuously varies with power level.

electrical-optical power difference, the lock-in amplifier, a compensation element, and the electrical heater. Note that the driver-heater is a non-linear element because its output power is proportional to its input voltage (V_D) squared. The transfer function of the lock-in amplifier contains several poles with characteristic frequencies on the order of $\omega = 15$. Consequently, if the compensation element is pure gain, the loop becomes unstable long before the gain is high enough to accurately balance the electrical and optical power. However, the loop can be stabilized by using a pure integrator for the compensation element. If the time constant of the integrator (τ_i) is sufficiently large, it will completely dominate the frequency response of the loop and the poles associated with the lock-in amplifier can be ignored. The integrator stabilizes the loop with a very high dc gain and also determines the system frequency response in a unique and desirable way. To see how this comes about, we can use figure 2.3 to derive an equation for the system response:

$$P_{elec} = \left\{ \frac{G_D G_P}{\tau_i} \int (P_{opt} - P_{elec}) dt \right\}^2 \tag{2.1}$$

After taking a square root and derivative on each side we have:

$$\frac{d\sqrt{P_{elec}}}{dt} = \frac{G_P G_D}{\tau_i} (P_{opt} - P_{elec}) \tag{2.2}$$

and finally this becomes:

$$\frac{d\ P_{elec}}{dt} = \frac{2\sqrt{P_{elec}}\ G_P G_D}{\tau_i} (P_{opt} - P_{elec}) \tag{2.3}$$

In the limit of small deviations from some equilibrium value of P_{elec}, $\sqrt{P_{elec}}$ is approximately constant and the solution of eq. (2.3) is a simple exponential with a time constant,

$$\tau_s = \frac{\tau_i}{2\sqrt{P_{elec}}\ G_P G_D} \tag{2.4}$$

The time constant automatically and continuously increases as the power decreases. Thus the system responds quickly at high power levels and achieves good sensitivity at low levels by increasing the time response which is equivalent to limiting the noise bandwidth. Since the loop gain is increasing steadily with power, the poles of the lock-in amplifier will eventually become important and cause instability. However, the integrator time constant can always be adjusted to put this instability threshold beyond the power capability of the system.

Although this nonlinearity of the servo loop is useful in determining the system time constant, it causes another problem when the system is operating near zero power. If for some reason the optical input is negative (e.g., when viewing a cold background) the system will attempt to drive negative electrical power by reversing the polarity of the heater voltage. However, since the heater output is proportional to V_D^2, the power is actually positive. In effect, the loop switches to positive feedback and will run away to saturation. This is easily prevented by clamping the heater voltage when it attempts to go negative. Then, however, when the optical input is negative the instrument will read a false zero. Thus measurements against a cold background will contain an offset which cannot be detected by making a zero measurement.

This problem is resolved by electronically offsetting the servo loop so that the electrical power always exceeds the optical power by some value P_{offset}. P_{offset} is then electronically subtracted from the display to make the instrument read correctly. Thus the system reads negative inputs up to the value of P_{offset}.

3. Circuit Design

Having outlined the major design decisions, we can now consider the specific circuits adopted to implement each of the blocks in figure 2.1. These circuits are intended to be a reasonable trade off between performance, simplicity, and cost. As new components become available, improvements will certainly be possible.

3.1 Chopper Speed Control

Since the detector preamplifier is tuned to a specific frequency ($\simeq$ 17 Hz) it is important that the chopper run at a precise speed. The circuit of figure 3.1 provides this speed control as well as supplying calibration and demodulation reference square waves.

The calibration reference is 180° out of phase with the optical signal and is used to turn the electrical calibration power on and off. The demodulation reference has an adjustable phase with respect to the optical signal and is used to synchronously rectify the output of the detector preamplifier.

The reference square waves are derived from an LED-phototransistor pick off which is intersected by the chopper wheel. The phase of this pick off is adjusted mechanically to be exactly 180° from the center of the optical aperture, thus providing the calibration reference. The demodulation reference is produced by delaying the calibration reference with a pair of one-shots.

The pick off is also used in the speed control to trigger a pulsing circuit. This circuit creates a stable 3 ms pulse whose height and width are independent of frequency. Thus, when the pulses are averaged, the resulting dc level is proportional to the chopper speed. This level is compared to a reference and the amplified difference signal drives the motor. This servo loop controls the chopper speed to better than 0.1 Hz.

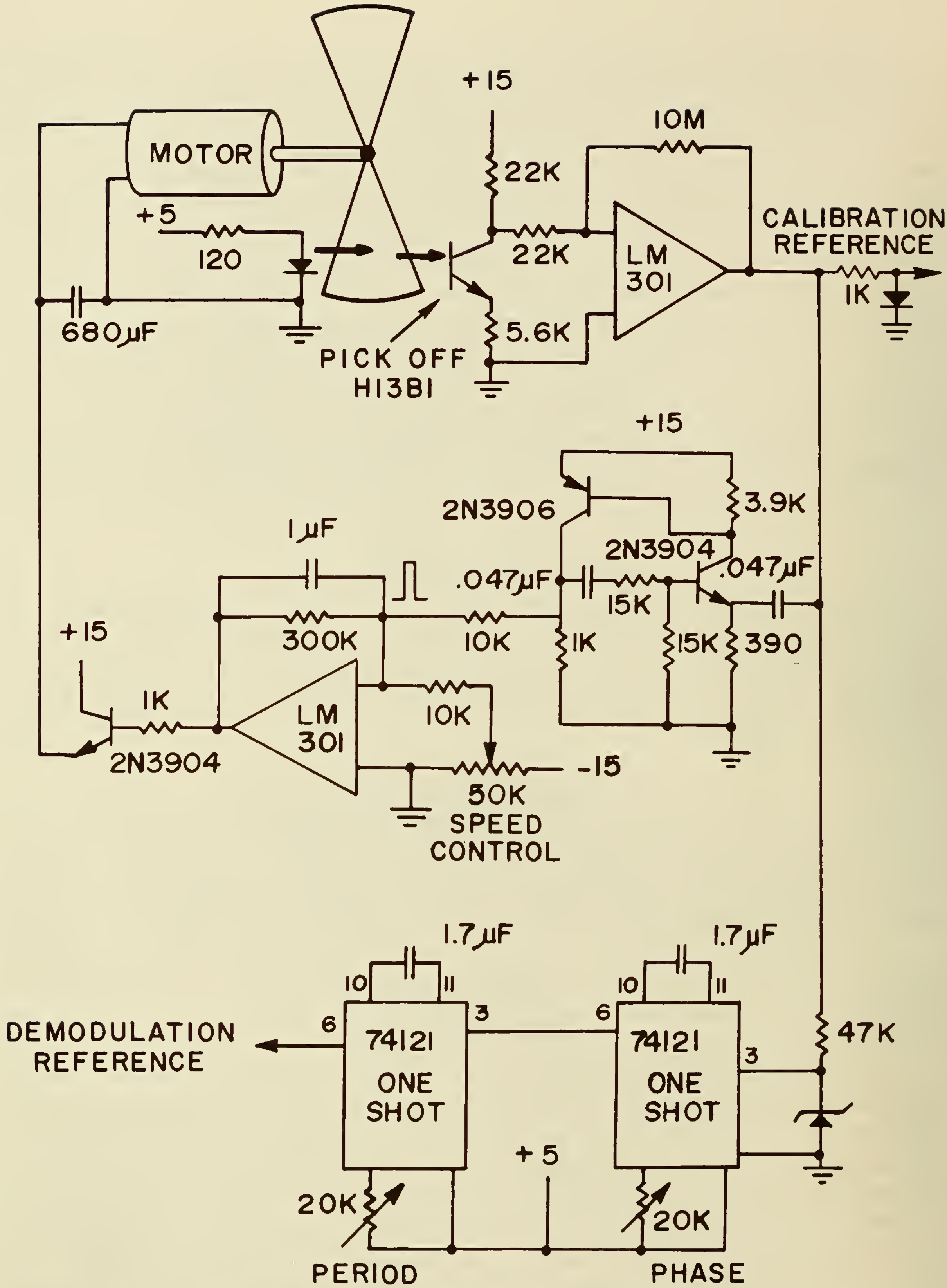

Figure 3.1 Chopper speed control schematic shows the derivation of the calibration and demodulation reference square waves.

3.2 Calibration Power Driver

Next we consider the circuit which produces the electrical calibration power. As was mentioned in section 2, the electrical calibration.power is driven by applying a voltage waveform like that shown in figure 2.2 across the detector heater. The circuit of figure 3.2 uses two inputs, a dc level, V_D, and the calibration reference square wave to produce the desired waveform. The operation is as follows: The reference square wave drives a flip flop producing a square wave at one half the reference frequency. This half frequency wave drives analog switch S1 which in turn switches the gain of amplifier A1 between +1 and -1. The output of A1 is thus a square wave varying between $+V_D$ and $-V_D$ at one half the chopper frequency. The reference square wave is also inverted and used to drive analog switch S2. S2 chops the output of A1 producing the desired waveform. Finally, the signal is amplified by two driver amplifiers which produce equal voltages of opposite polarity. These voltages are applied through an attenuator and standard resistor network to either end of the detector heater. The result is a symmetrical heater drive in which there is a virtual ground established at the center of the heater. The symmetrical drive, together with the alternating drive polarity, causes cancellation of any signals which are capacitively coupled from the heater to the detector output.

The 1000 pF capacitor in the drive circuit slows both drivers to a 0.2 ms rise time in order to eliminate switching transients. The effect of this slowed rise time on the electrical optical equivalence is examined in section 4 and shown to be negligible.

The gain of the driver-heater (G_D) can be calculated directly from figure 3.2. Beginning with the definition of G_D in figure 2.3 we have

$$(G_D V_D)^2 = P_{elec} = \frac{V_h^2}{R_D} = \frac{V_D^2\left\{\frac{2\ R_D}{R_D+R_a}\right\}^2}{R_D} = \frac{4\ V_D^2 R_D}{(R_D+R_a)^2} \tag{3.1}$$

where $R_a = R_I + R_1 + R_2$. Solving for G_D we have

$$G_D = \frac{2\sqrt{R_D}}{R_D + R_a} \tag{3.2}$$

In order to match dynamic ranges, it is desirable that when the system is reading full scale on the top range (P_{em}), the driver input voltage, V_D, should also be at its maximum value (V_{Dm}). Therefore

$$P_{em} = (G_D V_{Dm})^2 = V_{Dm}^2 \frac{4\ R_D}{(R_D+R_a)^2} \tag{3.3}$$

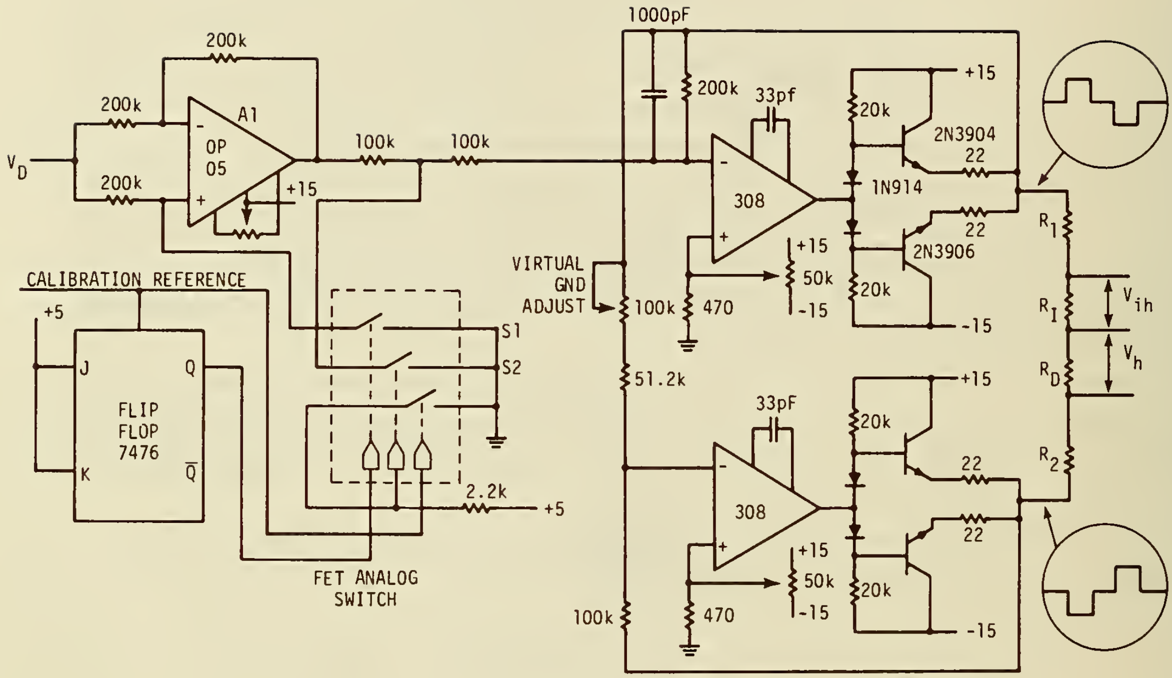

Figure 3.2 The calibration driver uses two inputs, V_D and calibration reference square wave to produce an alternating push-pull drive for the detector heater (R_D).

This equation is easily solved for R_a after which R_I, R_1 and R_2 can be selected to satisfy the virtual ground condition, i.e., $R_2 = R_1 + R_I$.

Finally, eq. (3.3) can be used to define a more general form of G_D, namely

$$G_D = \frac{\sqrt{P_{em}}}{V_{Dm}} \tag{3.4}$$

3.3 Auto Null Servo Loop

Having examined the operation of the mechanical chopper which modulates the optical input and the drive circuitry which modulates the calibration power, we can now consider the servo loop which automatically matches these two power levels. Figure 3.3 shows the detailed circuitry which makes up the servo loop shown as a block diagram in figures 2.1 and 2.3.

Before describing the circuit aspects of the loop, we must consider briefly the physics of the detector. Since the detector is a pyroelectric, its output current is proportional to the time rate of change of its temperature

$$I \propto \frac{dT}{dt} \tag{3.5}$$

Using an approximation appropriate for the low chopping frequencies in our system, the temperature derivative can be written as two terms, a positive term resulting from the power input and a negative term representing losses to the environment.

$$\frac{dT}{dt} = \frac{P}{C_p v} - \frac{T}{\tau} \tag{3.6}$$

Here $C_p v$ (heat capacity x volume) represents the thermal mass of the detector and τ is the inherent thermal time constant -- typically about one second. Since the chopping frequency (17 Hz) is considerably greater than $1/\tau$, the second term in eq. (3.6) can be considered constant and represents the average loss. Further, since the average power input must equal the average loss

$$\frac{dT}{dt} = \frac{1}{C_p v} (P-P_{ave}) \tag{3.7}$$

Thus the detector output is proportional to the difference between the instantaneous power and the average power. In the ideal case where the electrical and optical power inputs are square waves, 180° out of phase, the amplitude of the square wave detector output is exactly proportional to the power difference. Since the system normally nulls this difference, the lock in amplifier connected to the detector can have a very high gain and a considerably smaller dynamic range than the system as a whole. This is possible because the power difference is taken in the detector rather than in the lock in amplifier.

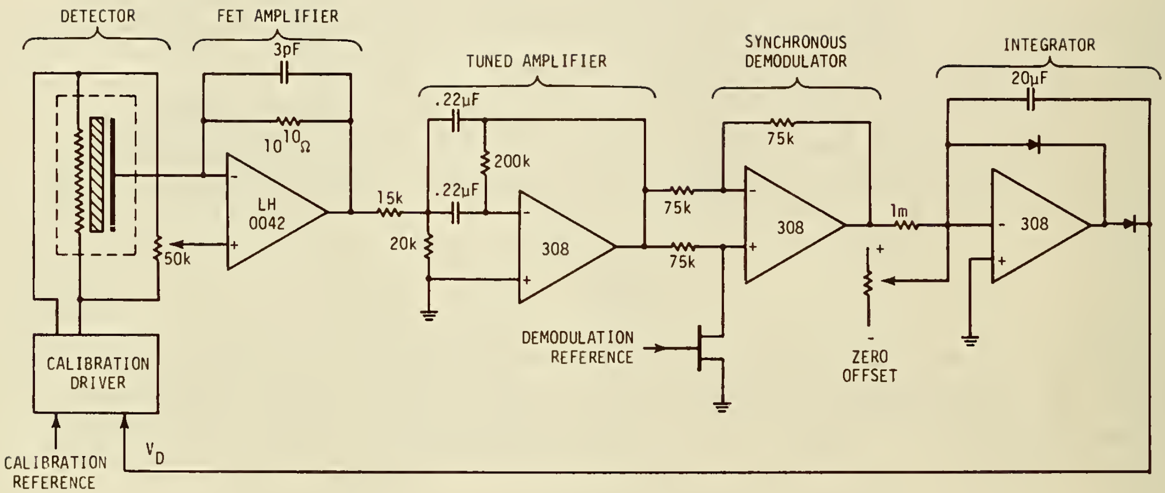

Figure 3.3 Schematic diagram of the detector, preamplifier and the null balance loop.

Returning now to figure 3.3, the detector output is amplified by a band limited current mode, FET, operational amplifier. The second stage is tuned to the chopper frequency, f_c, and selects only the fundamental component of the detector output. Finally the signal is synchronously rectified and averaged by the integrating amplifier. The overall gain of the preamplifier including the detector is given by

$$G_p = \frac{4}{\pi^2} r_i Z_f G_t \text{ (V/W)} \tag{3.8}$$

where r_i = current responsivity of the detector in A/W,

Z_f = FET amplifier feedback impedance at f_c,

G_t = center frequency gain of tuned amplifier.

The constant factor $4/\pi^2$ results from averaging the rectified fundamental component of the detector output. Typical values are $R_i = 10^{-6}$A/W, $Z_f = 2 \times 10^9\ \Omega$, $G_t = 6$, and $G_p = 5 \times 10^3$ V/W.

The phase for the synchronous rectifier is adjusted to 180° for the calibration signal and to 0° for an optical signal centered on the chopper aperture. The integrator output feeds the calibration power driver thus closing the loop. As mentioned in section 2, the integrator output is clamped to positive values and its input is offset by the equivalent of about a microwatt of optical power in order to allow the system to view negative background radiation.

In section 2 we showed that the system time constant, τ_s, is given by $\frac{\tau_i}{2\sqrt{P_{elec}}\, G_P G_D}$ and thus varies continuously in such a way that the S/N ratio is enhanced at low power levels. However, because of the heater nonlinearity, the system does not respond with a simple time constant to large changes in the input power. Consider the response to a large step function of optical power. In this case, both the system nonlinearity and the saturation level of the preamplifier become important. If the step function is large enough to saturate the preamplifier (P_{sat}), it will apply a constant voltage V_{pm} to the integrator. The integrator output then rises linearly causing the calibration power to rise parabolically. This continues until the preamplifier comes out of saturation after which the system approaches equilibrium exponentially with a time constant (τ_s) determined by the power level. These results are summarized in figure 3.4(a) which shows the system step response to a number of power levels and in figure 3.4(b) which shows τ_s and the system settling time (99%) as a function of power level. Both curves in figure 3.4(b) level out when the applied power level becomes small compared to the offset power. (See section 2.)

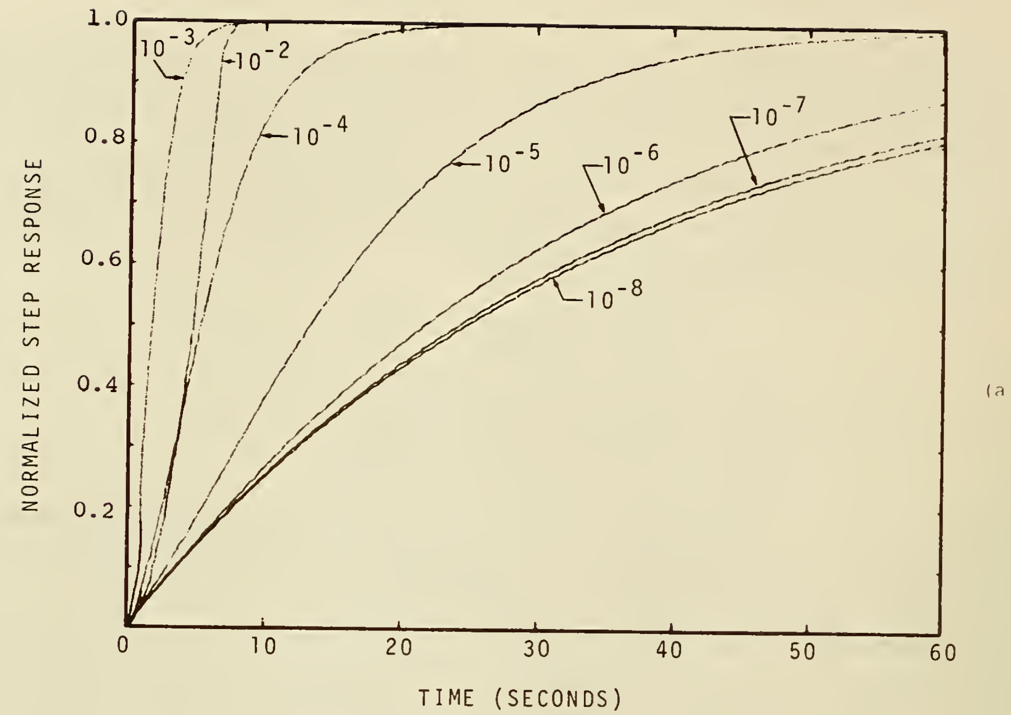

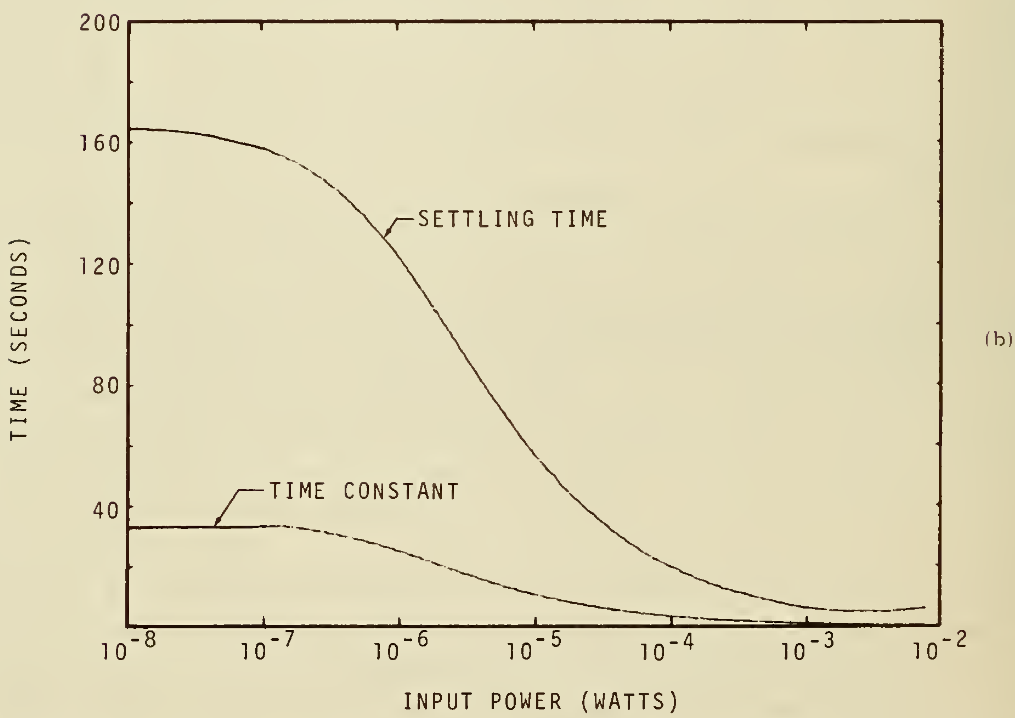

Figure 3.4 (a) Normalized system step response for power levels from 10^{-8} to 10^{-2} watts and (b) system settling time (99%) and small signal time constant as a function of power level.

The settling time decreases to a minimum at an input power equal to P_{sat}. For values above P_{sat}, saturation of the preamplifier in effect reduces the loop gain causing the settling time to increase.

Since the detector preamplifier is tuned to the chopper frequency and the synchronous rectifier has its phase set to zero (the phase of the electrical calibration power), the servo loop matches the fundamental, zero phase components of the optical and electrical signals. If the optical distribution over the chopper aperture is assymmetric, the optical signal will have a component which is 90° out of phase. Although this signal is rejected by the synchronous rectifier, it must not be allowed to saturate the preamplifier if the servo loop is to be effective. Since the in phase component is normally nulled, the out of phase component is the main cause of saturation and is thus the primary consideration in choosing the preamplifier gain. We can analyze this situation by taking the worst case optical distribution, i.e., a narrow beam at the aperture edge. This gives a square wave signal with a fundamental frequency component given by:

$$\frac{P_o 2}{\pi} \sin(\omega_{ct}+\theta) = \frac{P_o 2}{\pi} \{\cos\theta \sin\omega_{ct} + \sin\theta \cos\omega_{ct}\} \tag{3.9}$$

where P_o is the optical power and 2θ is the width of the aperture relative to the chopper center. The out of phase component has a value $\frac{P_o 2}{\pi} \sin\theta$. If the saturation value of the preamplifier output voltage is V_{sat}, then

$$P_{em} \sin\theta \leq \frac{V_{sat}}{G_p} = P_{sat} \tag{3.10}$$

For example, in a system with a 12 cm diameter chopper blade and a 1.25 cm aperture ($\theta = 6°$, $\sin\theta \simeq 0.1$), P_{sat} cannot be less than 0.1 times the maximum allowable input power P_{em}. This condition defines the maximum preamplifier gain. For typical values of P_{em} = 20 mW and V_{sat} = 10 volts, G_p must be less than or equal to 5000 v/w.

Figure 3.5 shows the output of the synchronous demodulator for several different conditions at the detector input. The first two waveforms (1 volt/div) are the nonequilibrium saturated output just after a positive going and a negative going step of optical power. The last three (0.1 volt/div) are the equilibrium waveforms for a narrow beam at the left edge, center and right edge of the chopper aperture. Since the zero phase component is nulled, the last three waveforms show only the component which is 90° out of phase together with a small residual component at $f_c/2$. The $f_c/2$ component arises from a slight misadjustment of the virtual ground. See section 3.2.

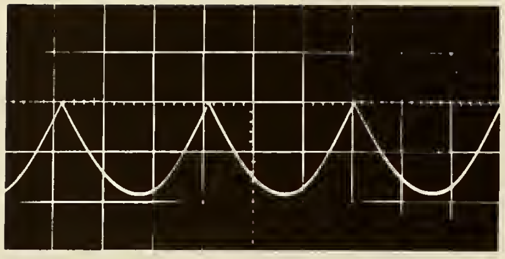

(A)

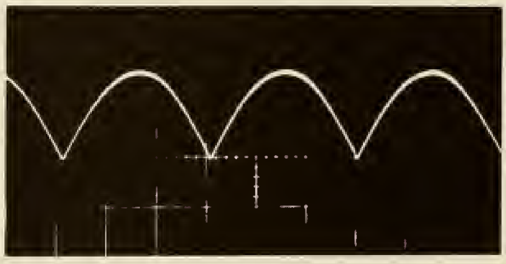

(B)

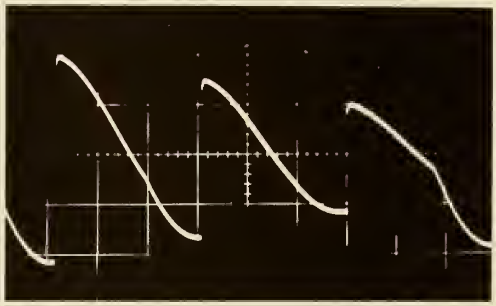

(C)

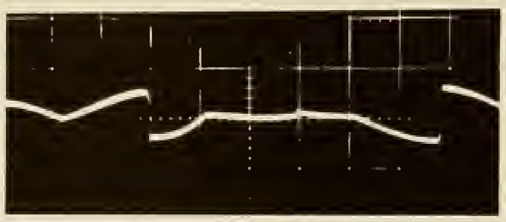

(D)

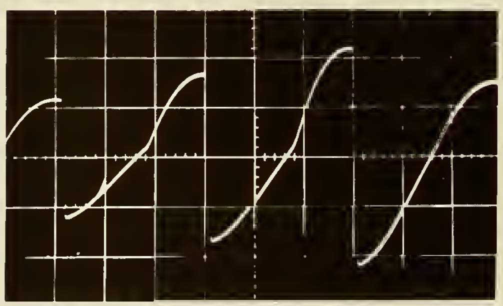

(E)

Figure 3.5 Waveforms at the synchronous demodulator output (a) just after a positive going step of optical power and (b) just after a negative going step of optical power. The last three waveforms are after the servo loop has reached equilibrium with a narrow optical input beam at the left edge of the chopper aperture (c), aperture center (d) and right edge (e).

3.4 Calibration Power Measurement

Figure 3.6 shows how the calibration power is measured. Two pairs of wires are connected to the detector heater, one to carry the current and the other to measure the voltage. A standard resistor in series with the detector heater current leads is used to measure the heater current. The voltage and current signals are amplified first with a pair of differential amplifiers and then by a pair of amplifiers which can be range switched between gain values of 1, $\sqrt{10}$, 10, and $\sqrt{1000}$. The two signals are then applied to a high precision, four quadrant, analog multiplier. The output of the multiplier is proportional to the instantaneous power dissipated in the detector heater. A filter after the multiplier samples the power during each heating cycle. This sampling is controlled by the calibration reference square wave. The sample time begins after the heater turn on transient has died out and ends before the heater is turned off.

The filtering between the multiplier output and the digital display is designed to provide at least 80 dB of attenuation at the chopper frequency, about 40 dB of attenuation at one half the chopper frequency, and yet still have a response time of less than a second. The 40 dB of attenuation at one half the chopper frequency, together with the alternating calibration drive voltage, has the effect of making zero offsets in the power drive and measurement circuits cancel out.

In order to compute the power correctly, the gains of the various stages in figure 3.6 must satisfy the following equation

$$\frac{R_4}{R_3 + R_4} \gamma G_V G_I R_I = \frac{V_{DPm(max)}}{P_{em}} \tag{3.11}$$

where γ = multiplier constant $\simeq$ .1,

G_V = differential voltage amplifier gain = R_5/R_6,

G_I = differential "current" amplifier gain = R_7/R_8,

R_I = standard current measuring resistor,

$V_{DPm(max)}$ = maximum voltage displayed on digital panel meter, and

P_{em} = maximum power displayed by system.

One additional constraint is necessary in order to match the voltage and current inputs to the multiplier:

$$R_I G_I \simeq R_D G_V \quad \text{(within ±20\%)} \tag{3.12}$$

where R_D is the detector resistance. When this condition is satisfied, the multiplier operates with maximum accuracy.

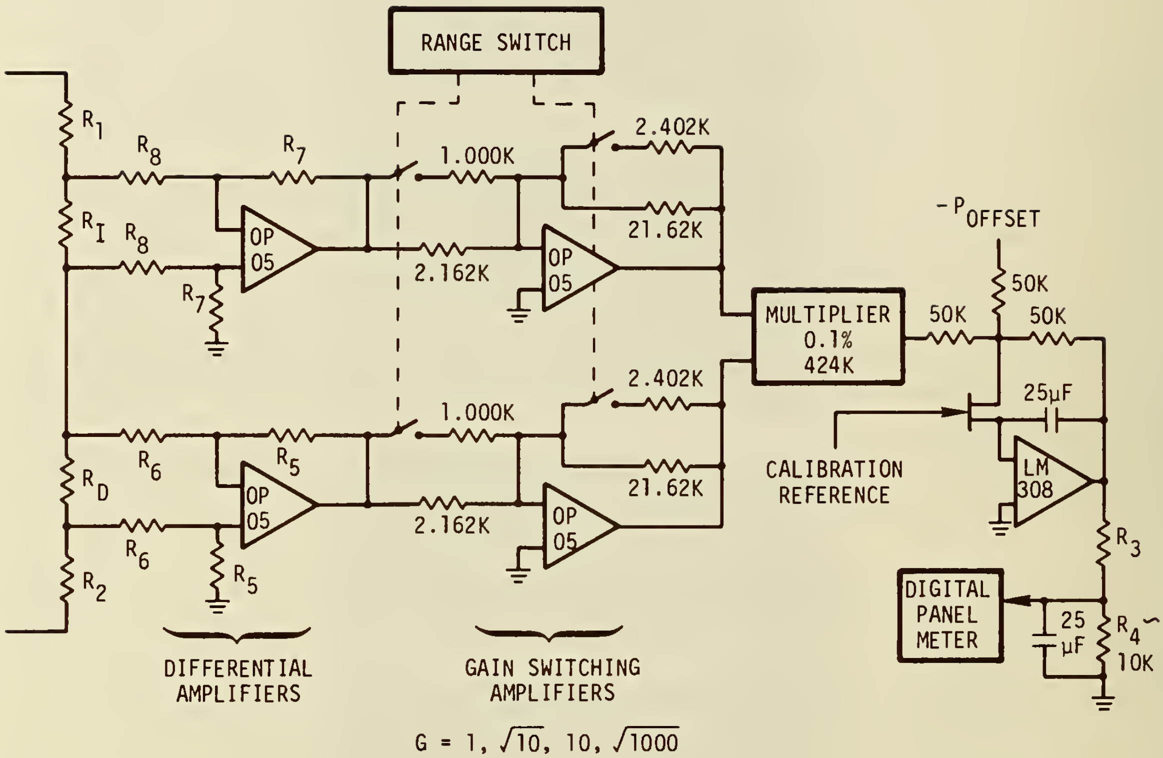

Figure 3.6 The power calculation circuitry uses high accuracy amplifiers and an analog multiplier to measure the power dissipated in the detector heater (R_D)..

In practice, eqs. (3.11) and (3.12) are used to select the various gains such that $\gamma \simeq 0.1$. γ is then adjusted experimentally to achieve calibration. This is accomplished by substituting a precision resistor for the detector heater and an on-off switch for the chopper. With the chopper switch in the "on" position, the displayed power (minus P_{offset}) is compared with V_h^2/R_D as measured with local laboratory standards. This comparison is made as an average over the positive and negative heater drive cycles. The accuracy and linearity of the power calculation circuitry are discussed in section 4.5.

4. Corrections and Error Analysis

The fundamental limitation on the accuracy of the ECPR is the extent to which the equivalence between electrical and optical power can be characterized. Although considerable effort has been devoted to producing equivalence, several small sources of inequivalence remain. Experimental procedures have been developed for estimating the magnitude of each of these sources of inequivalence. The total estimated inequivalence is used to internally correct the instrument reading. The uncertainty of these corrections is included in the error analysis. This section first describes the various corrections and then presents an error analysis of the complete system. It will be shown how each error source depends on the parameters of the system as well as the measurement conditions including power level, wavelength and irradiance distribution. The error estimates should be interpreted as one sigma values. Addition of errors is done in an rms fashion.

The final result is a curve of the total system uncertainty as a function of power level. It will be seen that the system accuracy is limited at the high power end by detector nonlinearity and at the low end by detector noise.

4.1 Irradiance Distribution

The previous sections have shown how the servo loop nulls the zero phase fundamental component of the electrical-optical power difference. In order to evaluate inequivalence which may result from this mode of operation, we must compare the fundamental component of the optical signal relative to its CW value, with the fundamental component of the calibration power relative to the value displayed on the digital panel meter. The waveform of the optical signal and therefore its fundamental component will depend on the irradiance distribution over the chopper aperture. For example, a narrow beam, when chopped, produces a square wave whereas uniform illumination of the chopper aperture produces a trapezoidal-like wave.

The results of a simple Fourier analysis for the electrical power waveform and for four different optical irradiance distributions are given in table 4.1. As before, 2θ is the angular width of the chopper aperture relative to the blade center, ω_c is the radian chopper frequency, and τ_c is the calibration driver risetime.

Table 4.1 Inequivalence resulting from electrical-optical waveform mismatch.

CW Power Arbitrary Units	Irradiance Distribution	Fundamental Component (V_f)	Value for a Typical ECPR[1]	Electrical-Optical Error
1.00 (Electrical)	--	$V_f = \frac{2}{\pi(1+\omega_c^2\tau_e^2)}$	$.9995 \frac{2}{\pi}$	
1.00 (Optical)	narrow beam at aperture center	$V_f = \frac{2}{\pi}$	$1.0000 \frac{2}{\pi}$	+.05%
1.00 (Optical)	uniform over aperture	$V_f = \frac{2 \sin n\theta}{\pi n \theta}$	$.9982 \frac{2}{\pi}$	-.13%
1.00 (Optical)	narrow beam at aperture edge	$V_f = \frac{2 \cos \theta}{\pi}$	$.9945 \frac{2}{\pi}$	-.50%
1.00 (Optical)	any distribution centered on aperture within ±50%	$\frac{2 \sin n\theta \cos(n\theta/2)}{\pi n \theta} < V_f < \frac{2}{\pi}$	$.9968 \frac{2}{\pi} < V_f < \frac{2}{\pi}$	-.11±.16%

[1] Design parameters used to arrive at the numerical values in the last two columns are:
Chopper aperture dimension = 1.25 cm
Chopper blade diameter = 12.00 cm
Number of blade openings n = 1
Chopper radian frequency ω_c = 110 sec^{-1} (17.5 Hz)
Calibration driver risetime τ_e = 200 µsec.

The worst case inequivalence occurs when the system views a narrow beam at the aperture edge. However, it is more reasonable to assume at least a crude alignment (±50%) and the last entry of table 4.1 shows the range of inequivalence which can occur based on this assumption. We shall use this value (−0.0011 ± 0.0016) for the analysis. Thus we have a required correction of +0.0011 with an uncertainty of ± 0.0016.

4.2 Detector Uniformity

For any thermal input, either electrical or optical, the detector output is proportional to the integrated product of the input power spatial distribution and the detector responsivity distribution. If the responsivity is nonuniform there may be an inequivalence between electrical and optical inputs. The magnitude of the inequivalence is given by

$$\varepsilon = \iint \{P_{elec}(X,Y) - P_{opt}(X,Y)\} r_i(X,Y) dx\, dy$$

where $r_i(X,Y)$ is the spatial distribution of responsivity. The electrical power distribution $P_{elec}(X,Y)$ is determined by the electrode geometry (see figure 1.1) and $P_{opt}(X,Y)$ may be any optical distribution within the input aperture. The inequivalence clearly depends on the size and position of the input beam as well as the uniformity of $r_i(X,Y)$. Figure 4.1(a) shows an analog uniformity scan of a typical detector. Such scans give a rapid but qualitative measure of the detector uniformity. A more quantitative value can be obtained by establishing a beam diameter consistent with the expected use of the instrument and measuring the responsivity at a large number of points on the detector surface. The results of such a determination on the same detector are shown in figure 4.1(b). The grid spacing is 0.75 mm and the beam diameter is approximately 1.0 mm ($1/e^2$ points). The results show a peak to peak deviation from the average of +.031 and −.026. These worst case points, however, are well away from the center of the detector. If the distribution of the input beam were known, the data of figure 4.1(b) could be used to calculate a correction factor. However, this is usually impractical and the nonuniformity is thus treated as a random error. The value of this error should be assigned based on the input beam characteristics and the uniformity data. In lieu of such a determination, a reasonable estimate is just the standard deviation of all of the points of figure 4.1(b). For this particular detector the value is ± 0.0125.

Another source of nonuniformity which must be considered is a depression of the responsivity around the whole perimeter of the active detector area. (The active area is that area of the pyroelectric material with both front and back electrodes.) This is caused by heat which is dissipated in the active area diffusing laterally into the inactive area. The diffusion distance is typically 30 μm in detectors made of PVF_2. Inequivalence from this source is avoided by preventing either electrical or optical power from being dissipated near the edges. The aperture performs this task for the optical power. The

(a)

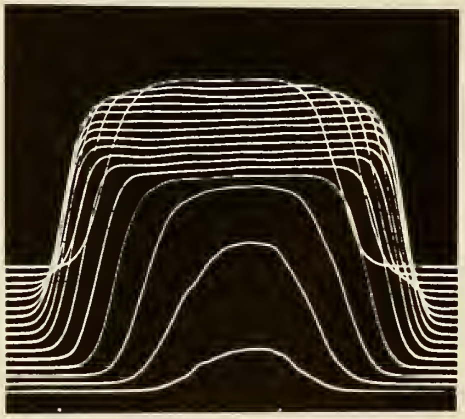

ANALOG
UNIFORMITY
SCAN

(b)

DIGITAL UNIFORMITY SCAN

-	-	1.008	1.008	1.008	1.002	0.991	0.984	-	-
-	1.016	1.007	1.009	1.003	1.000	0.993	0.992	0.974	-
1.019	1.016	1.005	1.004	0.999	0.994	0.991	0.988	0.974	0.980
1.018	1.012	1.007	1.010	1.001	0.996	0.991	0.986	0.978	0.985
1.022	1.017	1.013	1.015	1.006	1.001	0.996	0.992	0.988	0.988
1.031	1.023	1.011	1.006	1.003	1.002	0.997	0.993	0.998	0.993
1.027	1.020	1.014	1.007	1.002	1.004	0.996	0.996	0.998	0.990
1.019	1.016	1.014	1.002	0.993	0.986	0.990	1.001	0.991	0.988
-	1.011	1.006	0.997	0.992	0.990	0.989	0.998	0.983	-
-	-	1.005	0.999	0.993	0.988	0.991	0.994	-	-

Figure 4.1 Analog and digital uniformity scans of the detector response over its receiving surface.

problem is more difficult for the electrical power but can be solved for the most part by selecting an electrode geometry which concentrates the dissipation in the center of the detector. If this requirement was ignored and electrical power was dissipated uniformly over a 1 cm^2 detector, there would be an edge loss equal to the ratio of the 30 μm wide perimeter area to the total detector area or about 1%. The instrument would therefore read high by this amount and a correction would be required.

4.3 Detector Reflectance

Any optical power which is reflected from the gold black on the detector surface represents a direct inequivalence in the measurement. There are two methods of handling this. The first is to place the detector in a light trap which collects the reflected beam and returns it to the detector [7]. The second is to determine the total reflected power as a function of wavelength and make a correction. This determination can be made by measuring the spectral response of the detector versus a spectrally flat detector and then calibrating this response curve with one or more point measurements of reflectivity. The experimental setups used in these two determinations are shown in figure 4.2(a) and (b). The point reflectivity measurement (figure 4.2(a)) is made at a wavelength of 632.8 nm where the reflection is almost entirely diffuse. This diffuse reflection is detected with a large area annular pyroelectric detector of outside radius r_2 and a small center hole of radius r_1.

If the reflection is assumed to be Lambertian then the fraction of the reflected light which is intercepted by the annular detector is

$$\gamma = \sin^2\left\{\arctan \frac{r_2}{d}\right\} - \sin^2\left\{\arctan \frac{r_1}{d}\right\} \tag{4.2}$$

The separation distance d is chosen to maximize γ. Typical values are $r_1 = 0.075$ cm, $r_2 = 2.5$ cm, $d = 0.6$ cm and $\gamma = 0.94$. The reflectivity of the sample is determined by recording the annular detector output first with the sample in place (V_1) and then with a mirror of reflectivity η directing the entire beam back into the reflectometer (V_2). The reflectivity is then given by

$$\text{Reflectivity} = \frac{V_1\eta}{V_2\gamma} \tag{4.3}$$

Typical gold blacks show a reflectivity of about 0.0085 at $\lambda = 632.8$ nm when measured with this technique. The uncertainty in the reflectivity results mostly from nonuniformity and noise in the reflectometer and is estimated to be about ± 0.002.

The spectral response measurements are made using the system shown in figure 4.2(b). The output of the double prism monochromator is divided between the flat spectral response detector [7] (D#1) and the ECPR sample

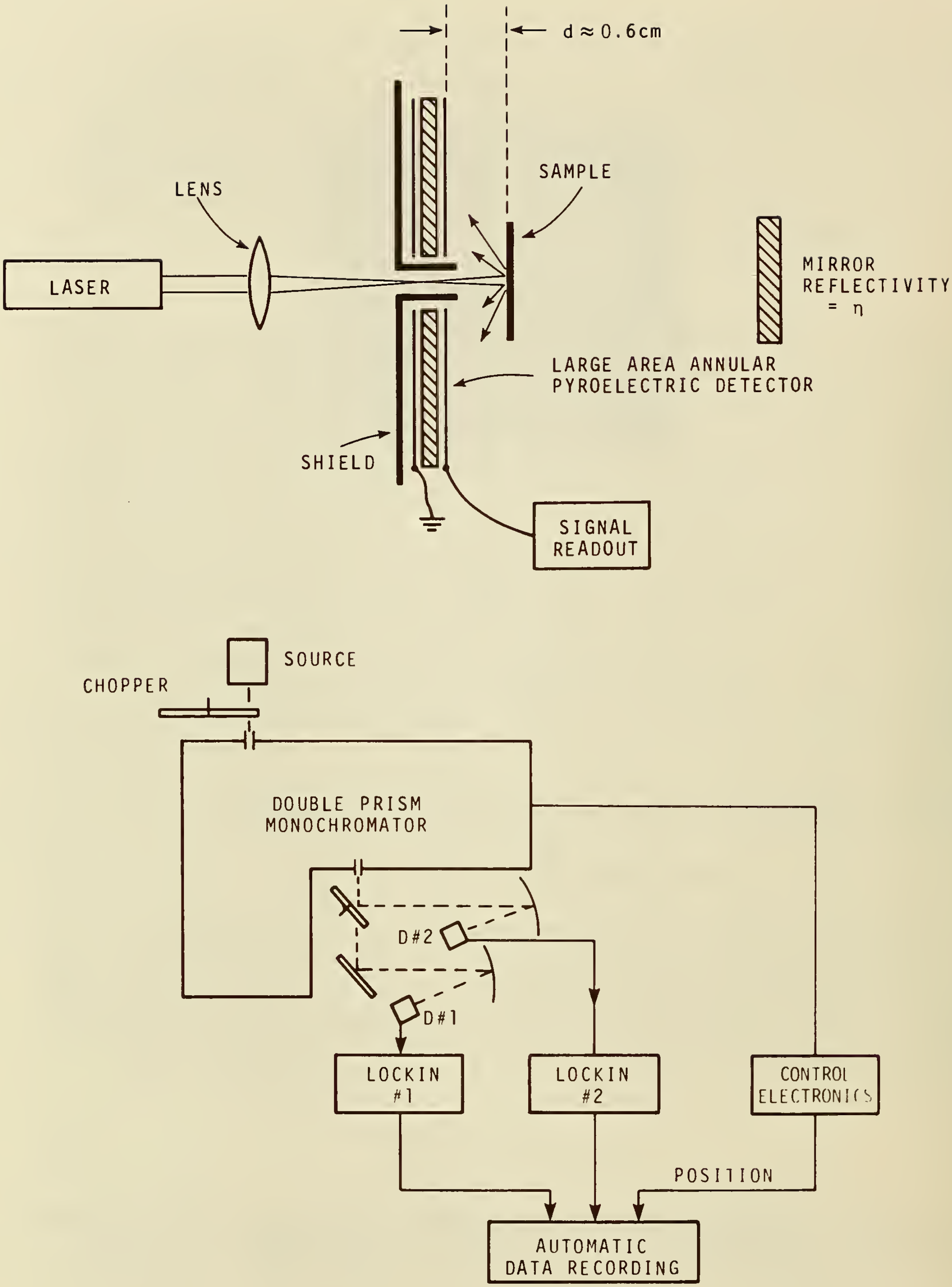

Figure 4.2 Spectral reflectance is determined by combining a point reflectance measurement (a) and a spectral responsivity measurement (b).

detector (D#2) with a rotating mirror chopper. The path lengths and time constants in the two channels are balanced. The output of the two detectors as well as the monochromator position are recorded on paper tape and processed with a minicomputer.

Spectral reflectance is determined by combining the spectral response and point reflectance measurements. Figure 4.3 shows a spectral reflectance curve for a typical gold black used on ECPR detectors. By changing the gold black deposition procedure, it is possible to achieve lower reflectance in the infrared. However, this usually results in a black which is more susceptible to damage and has a greater thermal resistance.

For an instrument which is to be used for visible light measurements, it is appropriate to make a fixed correction based on the relatively flat response over the visisble range. In the case of figure 4.3 the correction is +0.0085 with an uncertainty of ± 0.002.

4.4 Electrical-Optical Thermal Difference

The fact that the electrical and optical power are not dissipated at exactly the same position through the thickness of the black may lead to a slightly different detector response to the two inputs. A worst case analysis assumes that the optical power is absorbed at the front surface of the black and that the electrical power is dissipated under the black at the surface of the active detector material. Several experimental and theoretical analyses [10,11] have shown that for this worst case, the thermal conductance and capacitance of the black can lead to both a phase and amplitude difference between the electrical and optical signals. For typical blacks and chopping frequencies the dominant error mechanism is conduction to the air at the surface of the black. The optical input has a greater loss to the air because it is not impeded by the thermal resistance of the black. The magnitude of the difference varies from a few tenths percent to greater than one percent depending on the particular properties of the gold black used. Since these properties may vary widely from one black to the next, it is desirable to make a measurement for each black which is to be used in a calibrated system.

The theoretical analyses [10,11] show that by measuring the phase difference in the detector output between heat applied at the front and back surface of the black, both the thermal resistance and capacitance of the black can be obtained. These parameters, together with the known thermal properties of air, can be used to determine the difference in detector response to the two different heat inputs.

The apparatus of figure 4.4 is used to measure the phase difference as a function of frequency. The chopped laser beam is applied first to the black and then to an area where the black has been removed. In each case, the chopper is mechanically positioned with a micrometer mount to null the lock-in

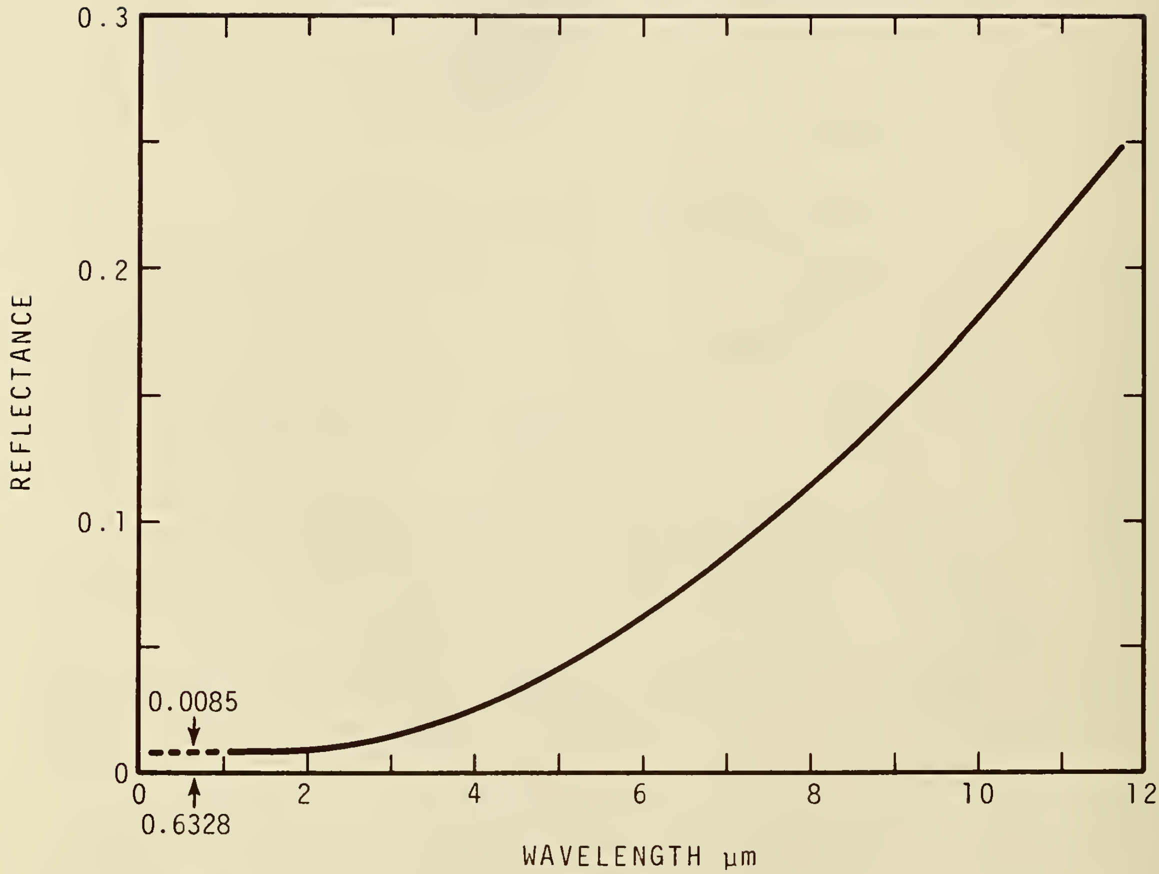

Figure 4.3 The spectral reflectance of a typical gold black.

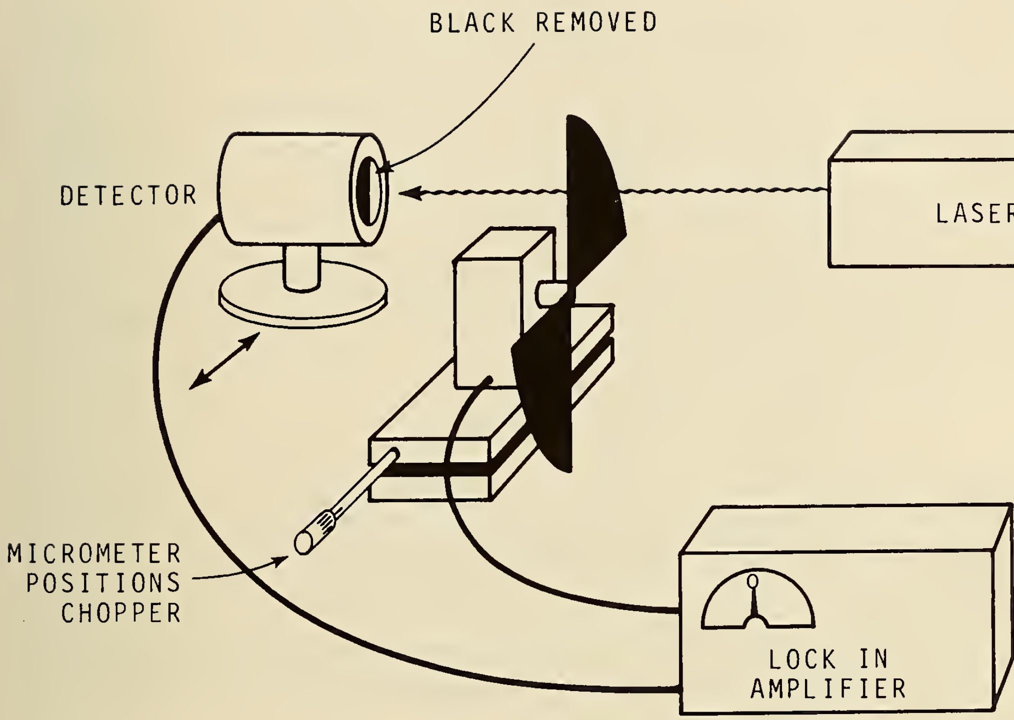

Figure 4.4 The thermal properties of the gold black are determined by measuring the phase shift in the detector response caused by the thermal delay through the black.

output. The difference in micrometer readings together with some simple geometry yields the phase difference. The phase resolution of this method is better than 0.1 degree.

The data obtained in this way are then fitted to an equation of the form

$$\Delta\phi = a_1\sqrt{f} + a_2 f \tag{4.4}$$

The approximate values [12] of the thermal resistance and capacitance of the black are given by

$$R_b \simeq \frac{a_1}{K_a\sqrt{\pi/\kappa_a}} = 0.1\ a_1 (W^{-1}Km^2) \tag{4.5}$$

$$C_b \simeq \frac{a_2}{\pi\ R_b}\ (J\ m^{-2}K^{-1}) \tag{4.6}$$

where K_a = air thermal conductivity = .026 $Wm^{-1}K^{-1}$,
κ_a = air thermal diffusivity = $2.1\times10^{-5}\ m^2S^{-1}$.

Finally, the ratio of the detector response to the heat at the front versus the back surface of the black is given by

$$\left|\frac{i_{back}}{i_{front}}\right| = \frac{1 + R_b(H_a+K_a\alpha_a)}{\cos\ \Delta\phi} \tag{4.7}$$

where H_a = radiation loss (near 300 K ambient) = 5.7 $Wm^{-2}K^{-1}$,
α_a = reciprocal of thermal diffusion distance of air = $\sqrt{\pi f_c/\kappa}$,
$\Delta\phi = a_1\sqrt{f_c} + a_2 f_c$.

The precision of the phase shift measurements and curve fitting suggest an overall accuracy for the determination of i_{back}/i_{front} of about ±0.4%. The results obtained on our typical black are

R_b = 270 μK $W^{-1}m^2$
C_b = 0.147 J $m^{-2}K^{-1}$
$\Delta\phi$(17.5 Hz) = 0.8°
i_{back}/i_{front} = 1.013 ± .004

This black was deposited at a nitrogen pressure of 230 P_a (1.73 torr), 8 cm from the source, and had a surface resistance of approximately 50 Ω/square.

Unfortunately, this method does not quite fit the actual situation in our electrically calibrated detector because the electrical power is dissipated more or less uniformly through the thickness of the black rather than all at the back surface. One would therefore expect the inequivalence to be only about one half as great. We therefore make a correction of +0.007 with an uncertainty of ± 0.004.

Another method of measuring the thermal inequivalence is to place the detector in a vacuum thus eliminating the heat loss to the air. However, the thermal resistance, R_b, of the diffuse gold black layer is highly dependent on the gas in which it is immersed. In a vacuum, R_b will increase resulting in an unknown increase in the radiation loss.

4.5 Lead Resistance

Resistance in the leads attached to the detector heater can cause two types of inequivalence. The first results from the heat caused by power dissipation in the current lead resistance. Some of this heat may reach an active area of the detector and add to the pyroelectric signal. The second type of inequivalence results from the fact that the voltage leads may not measure precisely the "effective" voltage across the heater. This effective voltage, V_{he}, is the difference of the average voltage distributions across either edge of the heater. It can be measured by applying a steady current through the heater and probing the voltage at about ten equally spaced points along either edge of the heater. The inequivalence resulting from the voltage measurement then is

$$\frac{V_{he} - V_h}{V_{he}} \qquad (4.8)$$

A typical value for this ratio is $-.004 \pm .001$. It can be reduced considerably by making the gold film on the lead pad area thicker.

The inequivalence resulting from lead heating can be determined by probing the voltage difference between the detector heater current leads, V_{ih}, and by measuring optically the responsivity of the lead pad area r_{ip} (see figure 1.1). The lead heating inequivalence then is

$$\frac{(V_{ih}-V_{he})}{V_{he}} \frac{r_{ip}}{r_i} \qquad (4.9)$$

Typical values are $r_{ip}/r_i < 0.1$ and $(V_{ih}-V_{he})/V_{he} \approx .008$ which yields an inequivalence of $+0.0008 \pm 0.0008$. The correction for both the voltage measurement and the lead heating inequivalence then is $+0.0032$ with an uncertainty (rms addition) of ± 0.0013.

4.6 Implementing Corrections

A summary of the principal corrections together with typical values is shown below:

	Correction
Irradiance Distribution	+0.0011 ± 0.0016
Detector Uniformity	0 ± 0.0125
Reflectivity (Visible Spectrum)	+0.0085 ± 0.002
E/O Thermal Difference	+0.0070 ± 0.004
Lead Resistance	+0.0032 ± 0.0013
Total Correction	$\varepsilon_c =$ +0.0198

A simple method of making the correction is to add a resistor, R_c, in parallel with the detector heater terminals. Some of the measured electrical power will be diverted to this resistor causing the instrument to read high. Precise compensation is achieved by choosing R_c such that $R_c = -R_D/\varepsilon_c$ where ε_c is the total correction to be made. The correction resistor is placed in parallel with the 50 K pot of figure 3.3 such that the combination yields the desired value.

4.7 Electrical-Optical Duty Cycle Difference

Although the electrical calibration power is switched by an LED-phototransistor pick off on the chopper blade, it may not have precisely the same duty cycle as the optical signal. This difference in duty cycles arises because the LED emits a beam which is several degrees wide relative to the chopper blade center. The actual switch point may occur anywhere in this several degree wide region and it is generally not symmetrical between the turn-on and turn-off points. For a typical chopper the difference may be as much as ±7°.

Fortunately, the fact that the system responds only to the fundamental component of the electrical and optical signals greatly reduces the effect of a duty cycle difference. Using Fourier analysis, we find that a duty cycle difference between the electrical and optical signals of β degrees results in a difference in fundamental components of $1 - \cos \beta/2$. Thus, assuming a worst case duty cycle difference of $\beta = \pm 7°$, the resulting fractional system error is ± 0.00187.

4.8 Detector Noise Error

All of the remaining errors are a function of the applied power level. The first of these is the fluctuation in the displayed power level which results from detector noise. The rms fluctuation, ΔP, of the displayed power from its expected value, P, is a function of the detector noise power spectral density at the chopper frequency, $P_N(f_c)$, and the small signal system time constant τ_s. τ_s in turn is a function of the applied power (see eq. (2.4)).

Detector noise results from acoustic disturbances together with the Johnson noise in the pyroelectric material. It can be modeled as a white noise current source i_n(amps/$\sqrt{Hz}$) in parallel with an ideal detector. It is convenient to express the noise in terms of power by dividing i_n by the current responsivity. Thus

$$P_N = \frac{i_n}{r_i} \quad (\text{watts}/\sqrt{Hz}) \tag{4.10}$$

If we think of P_N as an input to the servo loop, then the resulting system error is just the rms fluctuation at the output caused by the noise at the input. The effect of the lock in amplifier and servo loop is to translate the detector noise in a narrow band around the chopper frequency down to zero frequency. The bandwidth is determined by the small signal system time constant τ_s. The rms fluctuation ΔP is thus given by

$$\Delta P = \left\{ \int_o^\infty P_N^2(f_c) \left| \frac{1}{1 + j2\pi f\tau_s} \right|^2 df \right\}^{1/2} \tag{4.11}$$

which reduces to

$$\Delta P = \frac{P_N(f_c)}{2\sqrt{\tau_s}} \tag{4.12}$$

Substituting eq. (2.4) for τ_s and expressing ΔP as a fractional error we have

$$\frac{\Delta P}{P} = \pm P_N(f_c) \sqrt{\frac{G_P G_D}{2\ \tau_i}}\ P^{-3/4} \tag{4.13}$$

Typical values are $P_N(17\ Hz) = 1 \times 10^{-7}\ W\ Hz^{1/2}$, $G_P = 5000$ v/w, $G_D = .014\ W^{1/2}\ V^{-1}$ and $\tau_i = 5$ s which yields $\frac{\Delta P}{P} = \pm 2.6 \times 10^{-7}\ P^{-3/4}$.

4.9 Nonlinearity Error

Measurements of responsivity vs. temperature show that PVF_2 pyroelectric detectors may have a temperature coefficient of as much as +0.5%/K at room temperature. Thus when the applied power level is sufficient to raise the temperature of the PVF_2 more than a few degrees, the response becomes nonlinear. The null balance method of equating electrical and optical powers will cancel the nonlinear effect only if the power density of the optical signal matches the power density of the electrical signal. Since this is generally not the case, the nonlinearity error must be considered.

We shall define a worst case in which the optical input is a narrow Gaussian beam of 2 mm diameter ($1/e^2$ points). This beam diameter is typical of the output of many HeNe lasers. Previous experimental studies [13] have shown that in this case the fractional error is given by

$$\frac{\Delta P}{P} = +\ell P \tag{4.14}$$

where ℓ has a value of about 10 W^{-1}. Thus a narrow beam at 1 mW results in an error of about +1%. If the beam is larger or if uniform illumination is used the error is considerably smaller.

4.10 Quantization Error

Since the instrument uses a digital readout, there is always an uncertainty of ± 1/2 least significant digit. The fractional error resulting from this uncertainty depends on the power level being displayed. This fractional error for a 3 1/2 digit meter is given as a function of power level in eq. (4.15). These results assume that the decade range switch is always set to read the maximum number of significant figures.

$$\frac{\Delta P}{P} = \frac{10^{-6}}{2RP} \text{ where } \begin{array}{ll} R = 0.1, & \text{for } 2\text{x}10^{-3} < P < 2\text{x}10^{-2} \\ R = 1.0, & \text{for } 2\text{x}10^{-4} < P < 2\text{x}10^{-3} \\ R = 10.0, & \text{for } 2\text{x}10^{-5} < P < 2\text{x}10^{-4} \\ R = 100, & \text{for } \qquad\qquad P < 2\text{x}10^{-5} \end{array} \tag{4.15}$$

4.11 Power Calculation Error

Once the auto null servo loop has matched the electrical and optical powers, the electrical power must be computed and displayed. The circuitry for accomplishing this is described in section 3.4. There are three principal sources of error in the computation: 1) zero drift in the various amplifiers before the multiplier, 2) gain inaccuracy in the range switching amplifiers, and 3) nonlinearity in the multiplier module. The gain of the range switching amplifiers is determined by selected precision resistors and is accurate to 0.2%. The multiplier has a nonlinearity specification of 0.04% of full scale. Since the multiplier output is not normally less than an eighth of full scale we can assign a conservative error of 0.3% to the multiplier nonlinearity.

The errors caused by zero offsets are greatly reduced by the alternate polarity drive method (see Section 3.3). We can see how this comes about by evaluating the error resulting from a cumulative zero offset (referred to the output) of ΔV volts. The displayed power is the average over a positive and negative drive cycle, i.e.,

$$P_{display} = \frac{P_{em}}{V^2_{max}} \; \frac{(V+\Delta V)^2 + (V-\Delta V)^2}{2} \tag{4.16}$$

where V is the voltage appearing at the multiplier terminals and V_{max} is the value of V when the electrical power is at its maximum value P_{em}. If we define ΔP as the difference between the actual power ($P = P_{em} V^2/V^2_{max}$) and the displayed power, eq. (4.16) reduces to

$$\frac{\Delta P}{P} = \frac{\Delta V^2}{V^2} = \frac{\Delta V^2 \; P_{em}}{V^2_{max} \; P} \tag{4.17}$$

The numerical value of ΔV is the rms summation of eight different potential offsets in the driver and calculation circuitry. Each of these offsets is individually adjusted to less than 1 mV throughout the operating temperature range of the instrument. We therefore choose a value of ΔV of $\sqrt{8}$ mV. P_{em} is typically 20 mW and V_{max} is typically 7 volts.

The total power calculation error then is the rms summation over the three previously defined errors:

$$\frac{\Delta P}{P} = \pm\left\{(.002)^2 + (.003)^2 + \left(\frac{3\text{x}10^{-9}}{P}\right)^2\right\}^{1/2} \tag{4.18}$$

If the total offset should become excessive, it is easily observed as a significant (greater than 2%) difference between the power during positive and negative heater drive cycles during calibration. (See section 3.4 on the computation circuitry calibration procedure.)

4.12 Servo Gain Error

In any servo system the input-output error is the reciprocal of the loop gain. The ECPR is a so called type I system because the loop gain contains a single integration. Such systems in theory have infinite DC loop gain and therefore zero steady state input-output error. In fact, however, the integrator DC gain is limited by the leakage resistance of the feedback capacitor. The RC time defined by this leakage resistance is typically $\tau_\ell = 5000$ seconds. Thus the dc gain of the integrator $G_I = \tau_\ell/\tau_i$ or in our case $G_I \simeq 1000$.

The input-output error due to finite loop gain can now be computed by rewriting the loop eq. (2.1) with the integration operation replaced by G_I.

$$P_{elec} = \{G_P G_D G_I (P_{opt} - P_{elec})\}^2 \tag{4.19}$$

Rearranging and substituting our typical values we have

$$\frac{P_{opt} - P_{elec}}{P_{elec}} = \frac{1}{G_P G_D G_I \sqrt{P_{elec}}} = \frac{1.4 \times 10^{-5}}{\sqrt{P_{elec}}} \tag{4.20}$$

4.13 Error Summary

All of the previously described errors are summarized in table 4.2 and plotted as a function of power level in figure 4.5. The total system error is an RMS sum over all of these components. Two of the power dependent errors, the servo gain error and the nonlinearity error, have a known sign and are therefore added arithmetically and then put into the RMS summation. At the high power end, the accuracy is limited by detector nonlinearity while at the low end it is limited by detector noise. The best accuracy is achieved between 10 μW and 1 mW in a region where the error is dominated by detector nonuniformity.

As a result of the way the most significant errors have been evaluated, the total system error should be interpreted as a one sigma value, i.e., any given measurement has a 67% probability (confidence interval) of being within the stated accuracy. A 99% confidence interval can be obtained by multiplying the values of figure 4.5 by three. Thus, at a power level of 100 μW, the 99% confidence interval is ± 4%.

The nominal error values used for figure 4.5 correspond to the measurement of a 2 mm diameter Helium Neon laser beam at λ = 632.8 nm. Other types of measurements will lead to a different overall error. Two examples are compared with our nominal case in figure 4.6. Curve (b) corresponds to an irradiance measurement of visible light which uniformly illuminates the detector aperture. In this case the nonlinearity, nonuniformity and waveform errors are reduced and an error due to the uncertainty in the detector aperture area must be added. We have not considered the aperture area error in detail because it is not a fundamental part of the ECPR system. When applicable, this error must be determined for the aperture in use and added into the overall error.

Curve (c) shows the result for the measurement of power in a 2 mm beam from a 10.6 μm laser. In this case the uncertainty of the spectral response curve raises the overall error.

4.14 Failure Detection

In addition to all of the errors described so far, there are numerous failure modes which can cause abnormally large errors. In many cases the failure is obvious. For those failures which are not obvious, three simple tests will discover the problem in almost every case.

1) The use of the detector check button applies a preset current to the detector heater and displays the resulting power. Readings which are not consistent with the preset value (±5%) indicate a problem with the detector or power measurement circuitry.

Table 4.2 System errors.

Error	Nominal Value	Refer to Section
Correction Uncertainties		
Irradiance Distribution	$\pm\ 0.0016$	4.1
Detector Uniformity	$\pm\ 0.0125$	4.2
Detector Reflectance	$\pm\ 0.0020$	4.3
Thermal Equivalence	$\pm\ 0.0040$	4.4
Lead Resistance	$\pm\ 0.0013$	4.5
Duty Cycle	$\pm\ 0.0013$	4.7
Detector Noise[+]	$\pm\ 2.6\times10^{-7}P^{-3/4}$	4.8
Nonlinearity[+]	$+\ 10\ P$	4.9
Quantization	$\pm$ 1/2 least sig. digit	4.10
Power Calculation[+]	$\pm\ 10^{-3}[13+(3\times10^{-6}/P)^2]^{1/2}$	4.11
Servo Gain[+]	$-\ 1.4\times10^{-5}P^{1/2}$	4.12
Aperture Area	typically $\pm$ 0.001 when applicable	

[+] P is power in watts.

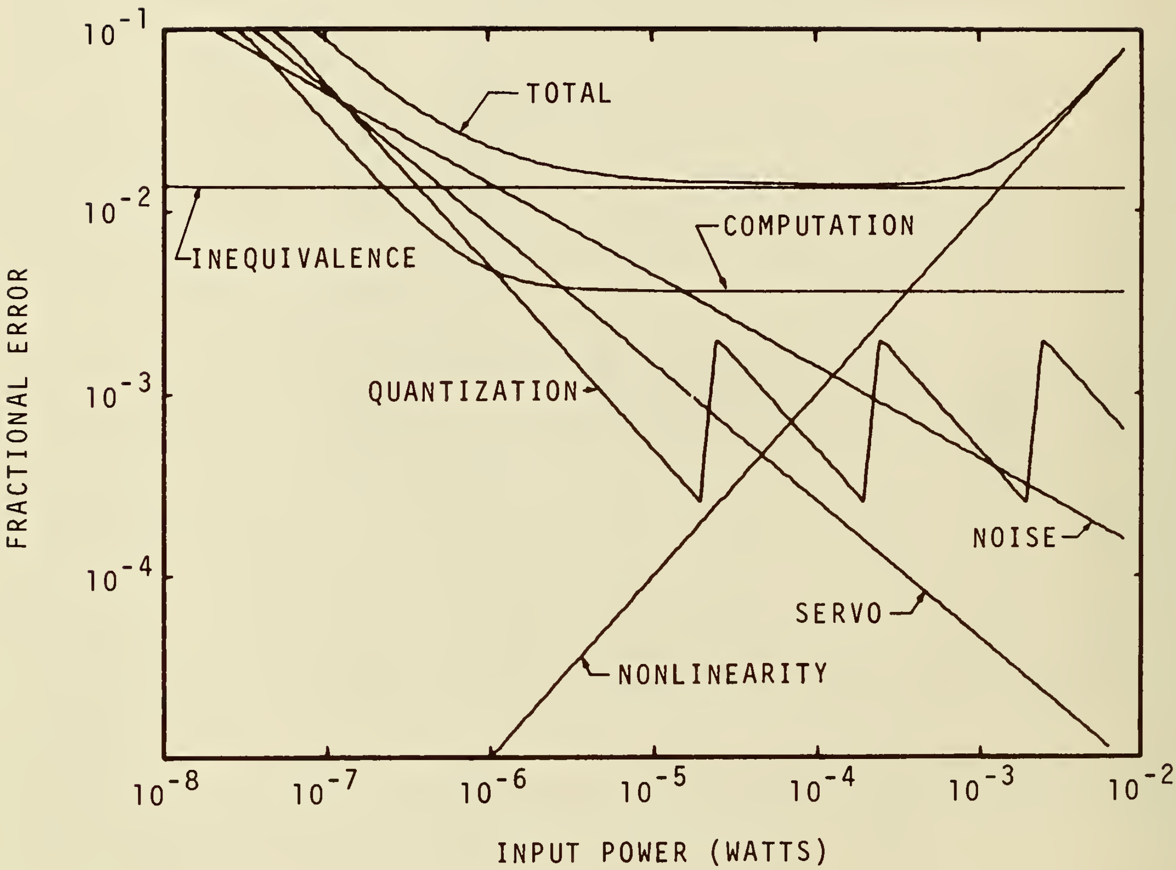

Figure 4.5 A plot of the random errors as a function of power level.

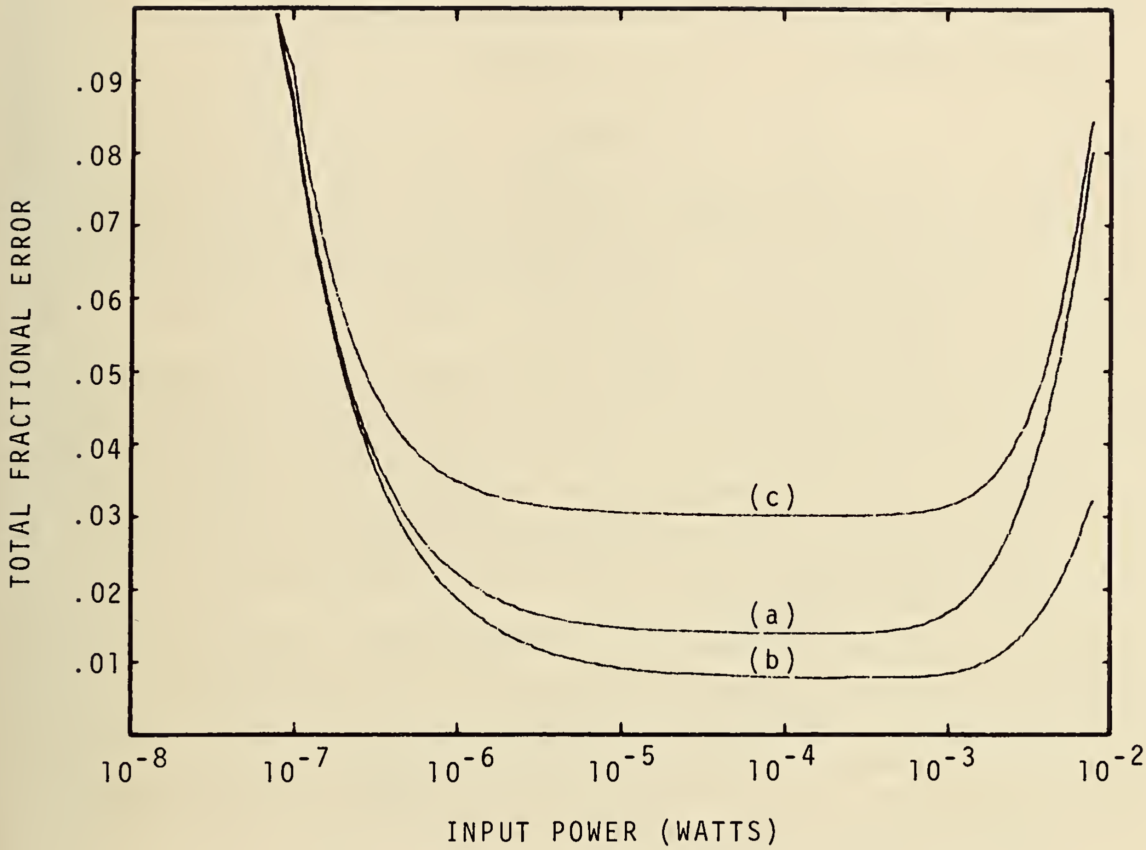

Figure 4.6 A plot of the total fractional error as a function of power level for three different types of measurement (a) a typical 2 mm diameter He-Ne laser beam (b) uniform visible illumination, and (c) a 10.6 µm CO_2 laser beam.

2) The electrical calibration procedure described in Section 3.4 should hold its accuracy to better than ± 0.3%. A difference of greater than 2% in the power reading between negative and positive drive cycles indicates a zero offset problem.

3) Using a beam diameter of about 2 mm, move the chopper aperture across the beam. The ECPR reading should peak with the beam centered and not decrease more than about 0.5% at either edge. A greater variation in the reading indicates a phase or chopper speed control problem.

5. Summary

The purpose of this Technical Note has been to describe in detail the design and analysis of an Electrically Calibrated Pyroelectric Radiometer. The results are sufficiently general that they can be applied not only to our particular instrument, but to a wide range of measurements involving electrically calibrated pyroelectric detectors.

In the error analysis we have tried to address all those errors which contribute in a significant way to the overall error in our system. The values which are given for the various errors are by no means a limitation but rather are examples of what has been achieved at this writing. Present systems are limited almost entirely by detector based errors. As improved technology reduces these errors, we can expect significant improvements in both accuracy and dynamic range.

The ECPR offers many advantages over more conventional radiometric measurement techniques involving standard sources. It is faster and simpler to use, and, most importantly, it results in a shorter and more direct measurement chain between the user and the basic standards. As these advantages are recognized, we believe the ECPR will become a widely accepted tool for accurate radiometric measurements.

Appendix A. Table of Symbols

C_b	heat capacity of gold black	J $m^{-2}K^{-1}$
C_p	heat capacity of pyroelectric material	J $m^{-3}K^{-1}$
f_c	chopper frequency	17.5 Hz
G_D	transfer function of calibration driver	.014 $W^{\frac{1}{2}}/V$
G_I	current measuring amplifier gain	
G_i	integrator dc gain	$\sim$ 1000
G_p	detector preamplifier gain	5000 VW^{-1}
G_t	center frequency gain of tuned amplifier	$\simeq$ 6
G_v	voltage measuring amplifier gain	
H_a	differential radiation loss at gold black surface	5.7 $Wm^{-2}K^{-1}$
I_p	pyroelectric current from detector	10^{-14} to 10^{-8} A
K_a	thermal conductivity of air	0.26 $Wm^{-1}K^{-1}$
ℓ	linearity error factor	10 W^{-1}
n	number of chopper blade openings	n = 1
P	optical and electrical power in system equilibrium	W
P_{elec}	electrical power dissipated in the "black"	W
P_{em}	maximum power to be measured by system	0.02 W
P_N	detector noise power spectral density	2×10^{-7} $W/\sqrt{Hz}$
P_{offset}	built in offset power $P_{elec} - P_{opt}$	$\simeq$ 1 μW
P_{opt}	optical power dissipated in the "black"	W
ΔP	a power uncertainty	W
$\left.\begin{matrix}R_1\\R_2\end{matrix}\right\}$	attenuation resistors calibration driver output	Ω
$\left.\begin{matrix}R_3\\R_4\end{matrix}\right\}$	voltage divider between multiplier output and digital panel meter	Ω
$\left.\begin{matrix}R_5\\R_6\end{matrix}\right\}$	differential voltage amplifier input and feedback resistors $G_V = R_5/R_6$	Ω
$\left.\begin{matrix}R_7\\R_8\end{matrix}\right\}$	differential current measuring amplifier input and feedback resistors $G_I = R_7/R_8$	Ω

R_a	$= R_I + R_1 + R_2$	Ω
R_b	thermal resistance of gold black	$W^{-1}K\ m^2$
R_c	error compensation resistor	Ω
R_D	detector heater resistance	20-60 Ω
R_I	standard resistor for current measurement	Ω
r_i	detector responsivity	$\simeq 10^{-6} AW^{-1}$
r_{ip}	responsivity of detector pad area	$< 0.1\ r_i$
T	temperature of pyroelectric material	K
t	time	S
V_D	voltage at input to calibration driver	0 to 10 V
V_{Dm}	maximum voltage at input to calibration driver	10 V
$V_{DPm(max)}$	full scale input voltage of digital panel meter	1.999 V
V_h	voltage across detector heater voltage sensing leads	V
V_{he}	effective voltage across detector heater	V
V_I	voltage at input to integrator	V
V_{ih}	voltage across detector heater current input leads	V
V_{sat}	saturation output voltage of preamplifier	$\simeq$ 10 V
ΔV	cumulative offset voltage of driver measurement circuit	V
v	volume of pyroelectric material	m^3
X, Y	spatial position over detector receiving surface	m
Z_f	feedback impedance on FET amplifier	$\simeq 10^9\ \Omega$
α_a	reciprocal of thermal diffusion distance in air	m^{-1}
β	angular difference between the electrical and optical duty cycles	
ε_c	total fixed error	
γ	electronic multiplier constant	$\simeq$ 0.1
θ	angular half width of chopper aperture relative to the blade center	
ϕ	phase difference between heat applied on front and back surface of black	
τ	detector thermal time constant	$\simeq$ 1 s

τ_e	calibration driver rise time (63%)	$\simeq 0.2$ ms
τ_i	integrator RC time	$\simeq 5$ s
τ_ℓ	capacitor leakage time constant	> 5000 s
τ_s	small signal system constant	s
ω	radian frequency	s^{-1}
ω_c	radian chopper frequency	s^{-1}
κ_a	air thermal diffusivity	$2.1\mathrm{x}10^{-5} m^2 s^{-1}$

References

[1] R.J. Phelan, Jr. and A.R. Cook, "Electrically Calibrated Pyroelectric Optical-Radiation Detector," Applied Optics, 12, 2494 (1973).

[2] Jon Geist and W.R. Blevin, "Chopper-Stabilized Null Radiometer Based Upon an Electrically Calibrated Pyroelectric Detector," Applied Optics, 12, 2532 (1973).

[3] R.J. Phelan, Jr., R.L. Peterson, G.P. Klein, C.A. Hamilton and G.W. Day, "Absolute, Pyroelectric Radiometers and Two Dimensional Arrays," Proceedings of the Electro-Optical System Design Conference, Sept. 18-20, 1973, New York, pp. 117-123.

[4] Jon Geist, "Fundamental Principals of Absolute Radiometry and the Philosophy of This NBS Program (1968 to 1971)," National Bureau of Standards Technical Note 594-1.

[5] Jon Geist, Bruce Steiner, Russell Schaefer, Edward Zalewski and Antonio Corrons, "Electrically Based Spectral Power Measurements Through the Use of a Tunable CW Laser," Applied Physics Letters, 26, 309 (1975).

[6] R.J. Phelan, Jr., "Electrically Calibrated Detectors Versus Black Body Sources," Proceedings of the IRIS Specialty Group on Infrared Detectors (March 1975).

[7] G.W. Day, C.A. Hamilton, and K.W. Pyatt, "A Flat Spectral Response Detector for the Visible to 12 μm Region," Proceedings of the IRIS Specialty Group on Infrared Detectors (March 1975).

[8] C.A. Hamilton and G.W. Day, "An Absolute Pyroelectric Radiometer (A Reference for Detector Responsivities)," Proceedings of the IRIS Specialty Group on Infrared Detectors (March 1975).

[9] Jon Geist, "Waveform-Independent Lock-In Detection," Review of Scientific Instruments, 43, 1704 (1972).

[10] W.R. Blevin and Jon Geist, "Influence of Black Coatings on Pyroelectric Detectors," Applied Optics, 13, 1171 (1974).

[11] R.L. Peterson, G.W. Day, P.M. Gruzensky and R.J. Phelan, Jr., "Analysis of Response of Pyroelectric Optical Detectors," Journal of Applied Physics, 45, 3296 (1974).

[12] Equations (4.3)-(4.5) are a simplification of eq. (32) from reference [10] based on the assumption of small error.

[13] C.A. Hamilton and G.W. Day, "A Pyroelectric Power Meter for the Measurement of Low Level Laser Radiation," National Bureau of Standards Technical Note 665.

NBS-114A (REV. 7-73)

U.S. DEPT. OF COMM. **BIBLIOGRAPHIC DATA SHEET**	1. PUBLICATION OR REPORT NO. NBS TN 678	2. Gov't Accession No.	3. Recipient's Accession No.
4. TITLE AND SUBTITLE An Electrically Calibrated Pyroelectric Radiometer System			5. Publication Date March 1976 6. Performing Organization Code 276.04
7. AUTHOR(S)			8. Performing Organ. Report No.
9. PERFORMING ORGANIZATION NAME AND ADDRESS **NATIONAL BUREAU OF STANDARDS** **DEPARTMENT OF COMMERCE** **WASHINGTON, D.C. 20234**			10. Project/Task/Work Unit No. 2764383 11. Contract/Grant No.
12. Sponsoring Organization Name and Complete Address *(Street, City, State, ZIP)* Same as Item 9.			13. Type of Report & Period Covered 14. Sponsoring Agency Code

15. SUPPLEMENTARY NOTES

16. ABSTRACT *(A 200-word or less factual summary of most significant information. If document includes a significant bibliography or literature survey, mention it here.)*

A new type of radiometer based on an electrically calibrated pyroelectric detector is described. Emphasis is placed on system design and analysis with careful consideration of design trade-offs. An evaluation of both systematic and random errors for the complete system yields an expression for the accuracy relative to the electrical standards by which it is calibrated. Throughout the paper the analysis should be sufficiently general that it can be applied to any Electrically Calibrated Pyroelectric Radiometer which employs the same basic principals.

17. KEY WORDS *(six to twelve entries; alphabetical order; capitalize only the first letter of the first key word unless a proper name; separated by semicolons)*

Detector; pyroelectric; radiometry.

18. AVAILABILITY [XX] Unlimited	19. SECURITY CLASS (THIS REPORT) UNCLASSIFIED	21. NO. OF PAGES 50
[ ] For Official Distribution. Do Not Release to NTIS [X] Order From Sup. of Doc., U.S. Government Printing Office Washington, D.C. 20402, SD Cat. No. C13.46:678 [ ] Order From National Technical Information Service (NTIS) Springfield, Virginia 22151	20. SECURITY CLASS (THIS PAGE) UNCLASSIFIED	22. Price $1.25

USCOMM-DC 29042-P74

☆ U. S. GOVERNMENT PRINTING OFFICE 1975 - 677-347/1259 Reg. 8

NBS TECHNICAL PUBLICATIONS

PERIODICALS

JOURNAL OF RESEARCH reports National Bureau of Standards research and development in physics, mathematics, and chemistry. It is published in two sections, available separately:

• **Physics and Chemistry (Section A)**

Papers of interest primarily to scientists working in these fields. This section covers a broad range of physical and chemical research, with major emphasis on standards of physical measurement, fundamental constants, and properties of matter. Issued six times a year. Annual subscription: Domestic, $17.00; Foreign, $21.25.

• **Mathematical Sciences (Section B)**

Studies and compilations designed mainly for the mathematician and theoretical physicist. Topics in mathematical statistics, theory of experiment design, numerical analysis, theoretical physics and chemistry, logical design and programming of computers and computer systems. Short numerical tables. Issued quarterly. Annual subscription: Domestic, $9.00; Foreign, $11.25.

DIMENSIONS/NBS (formerly Technical News Bulletin)—This monthly magazine is published to inform scientists, engineers, businessmen, industry, teachers, students, and consumers of the latest advances in science and technology, with primary emphasis on the work at NBS. The magazine highlights and reviews such issues as energy research, fire protection, building technology, metric conversion, pollution abatement, health and safety, and consumer product performance. In addition, it reports the results of Bureau programs in measurement standards and techniques, properties of matter and materials, engineering standards and services, instrumentation, and automatic data processing.

Annual subscription: Domestic, $9.45; Foreign, $11.85.

NONPERIODICALS

Monographs—Major contributions to the technical literature on various subjects related to the Bureau's scientific and technical activities.

Handbooks—Recommended codes of engineering and industrial practice (including safety codes) developed in cooperation with interested industries, professional organizations, and regulatory bodies.

Special Publications—Include proceedings of conferences sponsored by NBS, NBS annual reports, and other special publications appropriate to this grouping such as wall charts, pocket cards, and bibliographies.

Applied Mathematics Series—Mathematical tables, manuals, and studies of special interest to physicists, engineers, chemists, biologists, mathematicians, computer programmers, and others engaged in scientific and technical work.

National Standard Reference Data Series—Provides quantitative data on the physical and chemical properties of materials, compiled from the world's literature and critically evaluated. Developed under a world-wide program coordinated by NBS. Program under authority of National Standard Data Act (Public Law 90-396).

NOTE: At present the principal publication outlet for these data is the Journal of Physical and Chemical Reference Data (JPCRD) published quarterly for NBS by the American Chemical Society (ACS) and the American Institute of Physics (AIP). Subscriptions, reprints, and supplements available from ACS, 1155 Sixteenth St. N. W., Wash. D. C. 20056.

Building Science Series—Disseminates technical information developed at the Bureau on building materials, components, systems, and whole structures. The series presents research results, test methods, and performance criteria related to the structural and environmental functions and the durability and safety characteristics of building elements and systems.

Technical Notes—Studies or reports which are complete in themselves but restrictive in their treatment of a subject. Analogous to monographs but not so comprehensive in scope or definitive in treatment of the subject area. Often serve as a vehicle for final reports of work performed at NBS under the sponsorship of other government agencies.

Voluntary Product Standards—Developed under procedures published by the Department of Commerce in Part 10, Title 15, of the Code of Federal Regulations. The purpose of the standards is to establish nationally recognized requirements for products, and to provide all concerned interests with a basis for common understanding of the characteristics of the products. NBS administers this program as a supplement to the activities of the private sector standardizing organizations.

Federal Information Processing Standards Publications (FIPS PUBS)—Publications in this series collectively constitute the Federal Information Processing Standards Register. Register serves as the official source of information in the Federal Government regarding standards issued by NBS pursuant to the Federal Property and Administrative Services Act of 1949 as amended, Public Law 89-306 (79 Stat. 1127), and as implemented by Executive Order 11717 (38 FR 12315, dated May 11, 1973) and Part 6 of Title 15 CFR (Code of Federal Regulations).

Consumer Information Series—Practical information, based on NBS research and experience, covering areas of interest to the consumer. Easily understandable language and illustrations provide useful background knowledge for shopping in today's technological marketplace.

NBS Interagency Reports (NBSIR)—A special series of interim or final reports on work performed by NBS for outside sponsors (both government and non-government). In general, initial distribution is handled by the sponsor; public distribution is by the National Technical Information Service (Springfield, Va. 22161) in paper copy or microfiche form.

Order NBS publications (except NBSIR's and Bibliographic Subscription Services) from: Superintendent of Documents, Government Printing Office, Washington, D.C. 20402.

BIBLIOGRAPHIC SUBSCRIPTION SERVICES

The following current-awareness and literature-survey bibliographies are issued periodically by the Bureau:

Cryogenic Data Center Current Awareness Service

A literature survey issued biweekly. Annual subscription: Domestic, $20.00; foreign, $25.00.

Liquefied Natural Gas. A literature survey issued quarterly. Annual subscription: $20.00.

Superconducting Devices and Materials. A literature survey issued quarterly. Annual subscription: $20.00. Send subscription orders and remittances for the preceding bibliographic services to National Bureau of Standards, Cryogenic Data Center (275.02) Boulder, Colorado 80302.

Electromagnetic Metrology Current Awareness Service

Issued monthly. Annual subscription: $24.00. Send subscription order and remittance to Electromagnetics Division, National Bureau of Standards, Boulder, Colo. 80302.

U.S. DEPARTMENT OF COMMERCE
National Bureau of Standards
Washington, D.C. 20234

OFFICIAL BUSINESS

Penalty for Private Use, $300

POSTAGE AND FEES PAID
U.S. DEPARTMENT OF COMMERCE
COM-215

U.S.MAIL

Fourth Class Mail

AMERICAN REVOLUTION BICENTENNIAL 1776-1976

75 YEARS NBS 1901-1976